INSTITUTO POLITECNICO NACIONAL

Centro de Investigación en Ciencia Aplicada y Tecnología Avanzada Unidad Legaria

AN XPS STUDY ON THE COORDINATION MODE OF ORGANIC R-COO^{-} LIGANDS TO METAL CENTERS

TESIS

QUE PARA OBTENER EL GRADO DE

MAESTRO EN TECNOLOGÍA AVANZADA

P R E S E N T A

Lic. en Física Edgar Obed Pérez Reyes

CIUDAD DE MÉXICO Agosto, 2019

INSTITUTO POLITÉCNICO NACIONAL
SECRETARIA DE INVESTIGACIÓN Y POSGRADO

ACTA DE REGISTRO DE TEMA DE TESIS
Y DESIGNACIÓN DE DIRECTOR DE TESIS

Ciudad de México 30 de abril de 2019

El Colegio de Profesores de Posgrado de CICATA-Legaria en su Sesión
(Unidad Académica)

Ordinaria No. III celebrada el día 26 del mes marzo de 2019 conoció la solicitud presentada por el (la) alumno (a):

Apellido Paterno:	Pérez	Apellido Materno:	Reyes	Nombre (s):	Edgar Obed

Número de registro: B 1 7 0 6 5 8

del Programa Académico de Posgrado: Maestría en Tecnología Avanzada

Referente al registro de su tema de tesis; acordando lo siguiente:

1.- Se designa al aspirante el tema de tesis titulado:

An XPS study on the coordination mode of organic R-COO$^-$ ligands to metal centers

Objetivo general del trabajo de tesis:

Es el desarrollo de una metodología para identificar los modos de coordinación en superficie de ligantes R-COO$^-$ a centros metálicos por medio de la espectroscopía de fotoelectrones emitidos por Rayos X (XPS).

2.- Se designa como Directores de Tesis a los profesores:

Director: Dr. Oscar Fernando Odio Chacón 2° Director: Dr. Edilso Francisco Reguera Ruiz

No aplica: ☐

3.- El Trabajo de investigación base para el desarrollo de la tesis será elaborado por el alumno en:

CICATA-Legaria en el Laboratorio Nacional de Conversión y Almacenamiento de Energía (LNCAE)

que cuenta con los recursos e infraestructura necesarios.

4.- El interesado deberá asistir a los seminarios desarrollados en el área de adscripción del trabajo desde la fecha en que se suscribe la presente, hasta la aprobación de la versión completa de la tesis por parte de la Comisión Revisora correspondiente.

Director(a) de Tesis	2° Director de Tesis (en su caso)
Dr. Oscar Fernando Odio Chacón	Dr. Edilso Francisco Reguera Ruiz
Aspirante	Presidente del Colegio
Edgar Obed Pérez Reyes	Dra. Mónica Rosalía Jaime Fonseca

INSTITUTO POLITÉCNICO NACIONAL ESTADOS UNIDOS MEXICANOS
SEP
CENTRO DE INVESTIGACIÓN EN CIENCIA APLICADA Y TECNOLOGÍA AVANZADA
CICATA - LEGARIA

SIP-14
REP 2017

INSTITUTO POLITÉCNICO NACIONAL

SECRETARÍA DE INVESTIGACIÓN Y POSGRADO

ACTA DE REVISIÓN DE TESIS

En la Ciudad de México siendo las 12 horas del día 6 del mes de Junio del 2019 se reunieron los miembros de la Comisión Revisora de la Tesis, designada por el Colegio de Profesores de Posgrado de: CICATA-Legaria para examinar la tesis titulada: An XPS study on the coordination mode of organic R-COO- ligands to metal centers por el (la) alumno (a):

Apellido Paterno:	Pérez	Apellido Materno:	Reyes	Nombre (s):	Edgar Obed

Número de registro: B 1 7 0 6 5 8

Aspirante del Programa Académico de Posgrado: Maestría en Tecnología Avanzada

Después de la lectura y revisión individual, así como el análisis e intercambio de opiniones, los miembros de la Comisión manifestaron **APROBAR** ☒ **NO APROBAR** ☐ la tesis, en virtud de los motivos siguientes:

Satisface los requisitos señalados por las disposiciones reglamentarias vigentes.

Comisión Revisora de Tesis

Dr. Oscar Fernando Odio Chacón
(Director de Tesis)

Dr. Miguel Ángel Aguilar Frutis
(Presidente 11382-EE-15
Profesor Colegiado)

Dra. Ana Adela Lemus Santana
(Secretario 13099EC-18
Profesor Colegiado)

Dr. Edilso Francisco Reguera Ruiz
(2° Director de Tesis12103-EE-16
Profesor Colegiado)

Dr. Próspero Acevedo Peña
(Tercer Vocal)

Presidente del Colegio de Profesores

Dra. Mónica Rosalía Jaime Fonseca

INSTITUTO POLITÉCNICO NACIONAL
SEP
CENTRO DE INVESTIGACIÓN EN CIENCIA APLICADA Y TECNOLOGÍA AVANZADA
CICATA - LEGARIA

INSTITUTO POLITÉCNICO NACIONAL

SECRETARÍA DE INVESTIGACIÓN Y POSGRADO

CARTA CESIÓN DE DERECHOS

En la Ciudad de México el día 6 del mes Junio del año 2019, el que suscribe Edgar Obed Pérez Reyes alumno del Programa de Maestría en Tecnología Avanzada con número de registro B170658, adscrito al Centro de Investigación en Ciencia Aplicada y Tecnología Avanzada Unidad Legaria CICATA-Legaria , manifiesta que es autor intelectual del presente trabajo de Tesis bajo la dirección de Dr. Oscar Fernando Odio Chacón y de Dr. Edilso Francisco Reguera Ruiz y cede los derechos del trabajo titulado An XPS study on the coordination mode of organic R-COO-ligands to metal centers, al Instituto Politécnico Nacional para su difusión, con fines académicos y de investigación.

Los usuarios de la información no deben reproducir el contenido textual, gráficas o datos del trabajo sin el permiso expreso del autor y/o director del trabajo. Este puede ser obtenido escribiendo a la siguiente dirección edgarp656@gmail.com . Si el permiso se otorga, el usuario deberá dar el agradecimiento correspondiente y citar la fuente del mismo.

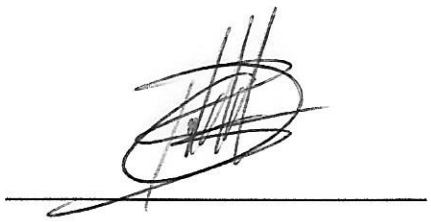

Edgar Obed Pérez Reyes

INDICE

SECTION	PAGE
LIST OF FIGURES……...	1
LIST OF TABLES……	3
ABSTRACT……	4
INTRODUCTION……..	5
CHAPTER I: STATE OF ART……	7
1.1 Physical basis of X-Ray Photoelectron Spectroscopy……...	7
1.1.1 Physical Basis…….....	7
1.1.2 XPS Line Shapes……	10
1.1.3 Chemical Shift……	11
1.1.4 Additional spectral lines……...	12
1.2 X-Ray Photoelectron Spectroscopy applied to coordination chemistry……	15
1.3 Coordination chemistry of metal carboxylates……..	16
1.4 Techniques and methods for the identification of metal carboxylates coordination modes……..	17
1.4.1 Nuclear magnetic resonance (NMR)……	17
1.4.2 Infra-Red Spectroscopy (IR)……...	18
CHAPTER II: EXPERIMENTAL SECTION……	20
2.1 Materials and Equipment……	20
2.2 XPS measurements……...	23
CHAPTER III: RESULTS AND DISCUSSION……	24
3.1 Experimental Characterization……..	24

3.1.1 Infra-Red Spectroscopy (IR)…… 24
3.1.2 X-Ray Photoelectron Spectroscopy (XPS)…….. 27
3.1.2.1 C1s Region……... 27
3.2.1.2 O1s Region…….. 30

CONCLUSIONS…… 34

ANEX A…….. 35

ANEX B……... 37

ANEX C…….. 38

REFERENCES……... 44

LIST OF FIGURES

Figure		Page
1	Schematic representation of photoemission process in an XPS experiment……..	6
2	Splitting energy level with an angular $l \neq 0$ arising to the spin-orbit coupling which give a higher energy when electron's spin is parallel to the magnetic moment and lower energy when is antiparallel ….....	7
3	Mg x-ray satellites observed in the C1s spectrum of graphite……	12
4	Cu 2p region for metallic cooper and cooper oxides. Metallic Cu does not exhibit satellite by other hand Cu(I) oxide present a weak satellite around 945 eV meanwhile Cu (II) Oxide has a strong satellite feature…..	13
5	Binding modes for metal carboxylates: a) Monodentate, b) Bridging Bidentate, c) Chelating, d) Ionic, e) Pseudo Bridging Bidentate, f) Bridging ($\mu_3\eta^1\eta^2$Mode), g) Chelating Bridging and h) Chelating Bridging ($\mu_3\eta^1\eta^2\eta^1$Mode)…….	15
6	Thermal decompositions diagrams of Zinc Acetate dihydrated Zn (CH3COO)2 2H2O (left) and Cu (CH3COO) H2O (right). Anhydrous phase of Zn (CH3COO)2 2(H2O) was obtained around of 80º Celsius degrees meanwhile the anhydrous phase of Cu (CH3COO)2 (H2O) was obtained around 108º Celsius degrees……	19
7	The so called Pseudo Bridging Bidentate. This binding mode is a monodentate geometry with an additional interaction, a hydrogen bond.	26
8	C-O bond lengths in the carboxylate group for Cu Ac NH3 (left) and Zn Ac 2H2O (right), both are chelating compounds but Cu Ac NH3 present a asymmetry in its carboxylate geometry…….....	28
9	C1s peak of metal acetates with different geometries: a) Ionic, b) Pseudo Bridging Bidentate, c) Bidentate and d) Chelating. Peak fitting show the assignment of CH3 and COO species, the remaining peaks (black line) were assigned to adventitious contamination species. C1s peak of COO group appear in different positions due to distinct chemical environments.....	30

10 C1s binding energy ranges for various coordination modes. Monodentate and ionic geometries tend to lower binding energies than Chelating, Bridging Bidentate and Pseudo Bridging Bidentate geometries……..... 31

12 O1s peak of metal acetates with different geometries: a) Chelating, b) Bridging Bidentate, c) Pseudo Bridging Bidentate, d) Monodentate and e) Ionic. Peak fitting show different chemical shifts for distinct coordination modes. Only in the Monodentate geometry is possible distinguish two types of oxygen atoms C-O-M and C=O…….. 33

13 O1s binding energy ranges for various coordination modes. Ionic and Pseudo Bridging Bidentate geometries present lower binding energies than chelating and bridging Bidentate. Monodentate geometry is characterized by the presence of two signals associated with oxygen atoms in C-O-M and C=O bonds…… 34

LIST OF TABLES

Table		Page
1	The relationship between quantum numbers and spectroscopists' notation……..	10
2	Model compounds studied here and their respective binding mode. From left to right: Pseudo Bridging Bidentate, Monodentate, Chelating, Bridging Bidentate, Bridging ($\mu_3\eta^1\eta^2$Mode), Chelating Bridging, Chelating Bridging ($\mu_3\eta^1\eta^2\eta^1$Mode) and Ionic…….	21
3	Infrared frequencies (cm^{-1}) of symmetric Vas (COO-) and symmetric Vsym (COO-) bans of different binding modes in transition metal carboxylates…….....	26
4	C1s and O1s binding energy for various coordination modes. Ionic and Pseudo Bridging Bidentate geometries present lower binding energies than chelating and bridging Bidentate. In the O1s Region Monodentate geometry is characterized by the presence of two signals associated with oxygen atoms in C-O-M and C=O bond…….....	37

ABSTRACT

This thesis is within the context of surface science, more specifically in the context of the structure of coordination compounds at the surface of materials, this is in order to unravel the mechanism of interfacial interactions between the surface atomic lattices and their surroundings. These interactions can be modified and tuned by surface functionalization, for example one of the most commonly used functional groups at the surface of materials are the metal carboxylates due to their versatility in the way that they can binded to the surface, which can change the surface properties. For this reason, they are of prime interest in hot topics such solar cells, catalysis and nanoengineering. Customary techniques like XRD and FTIR which are used to perform structural analysis are sensible to the bulk structure, but they provide poor information about the surface; on the contrary, XPS senses fundamentally the chemical environment and the behavior of surface atoms. In this work, we aim to employ XPS as an alternative technique to elucidate the coordination mode in transition metal carboxylates, by using several metal acetates as model compounds. Specifically, we show how the chemical shifts observed in the C1s and O1s signals of metal carboxylate in the XPS spectrum can be used to distinguish between common binding modes of metal carboxylates. All the conclusions presented in this work are supported by structural data obtained from X-Ray Powder Diffraction.

INTRODUCTION

Understanding chemical and physical interactions on the surface's materials is fundamental to the study of important processes like catalytic activity [1], adsorption [2], corrosion [3, 4] or charge transfer [5, 6]. These processes can be modified through surface functionalization using a suitable anchoring group [2, 7-10] . Carboxylate is a common ligand employed in wastewater treatment to removal metal ions [11, 12] and surface functionalization to change surfaces properties like chemisorption, hydrophobicity or charge transfer [2, 13-16]. It has been reported that the binding geometry is crucial in nanoparticle stabilization [13], photovoltaic efficiency in systems like dye-sensitized solar cells (DSSCs) [14, 17, 18], hydrophobic properties [16] and the selectivity of oxidation and ammoxidation reactions [2].

The coordination modes that are typically encountered in metal carboxylates; account for the traditional modes: monodentate, bridging bidentate and chelating and ionic behavior, there are additional modes that are a combination of the traditional modes. Several spectroscopic techniques have focused on the distinction of carboxylates coordination modes like Nuclear Magnetic Resonance (NMR), which associate the 13C chemical shifts of carbon atoms in the carboxylate group with the different binding modes of carboxylate complexes [19, 20] , Raman Spectroscopy [21, 22] and Infra-Red Spectroscopy (IR) [23], both Raman and IR spectroscopies have a similar methodology based in the magnitude of the separation between the frequency of asymmetric Vas (COO-) and symmetric Vsym (COO-) carboxylate vibration, $\Delta = V_{as}-V_{sym}$, as indicative of coordination geometry. In the IR spectra it has been reported that monodentate complexes present Δ values greater than ionic complexes, whereas chelating and bridging complexes have Δ values lower than ionic [23]. However, this relationship has to be carefully applied especially when very low Δ values appear since it could be indicate a combination of chelating and bridging [23] and when hydrogen bonds are present since in this situation it might not be possible distinguish between

bridging and pseudo bridging bidentate [23, 24]. On the other hand, the mentioned techniques have a poor surface resolution; this means that is more complicated to identify the surface carboxylate binding mode by using this kind of analysis. In this sense, X-ray photoelectron spectroscopy (XPS) could be helpful due to its high surface sensitivity (10-200 Å) and confident information about chemical bonding. Some reports have used XPS to determine the adsorption geometry of organic molecules containing carboxylic acids groups [15, 25, 26], but they lack of extensive analysis about the different binding geometries. Our work presents an XPS study of several transition metal acetates as model compounds for metal carboxylates, in order to propose guidelines for the distinction of representative carboxyl binding modes. Analysis are based in deconvolution of high-resolution spectra of C1s and O1s signals, and the results are correlated with structural data provided by X-ray powder diffraction (XRPD). The analysis performed here was supported with.

CHAPTER I: STATE OF ART

1.1 Physical basis of X-Ray Photoelectron Spectroscopy

X-Photoelectron Spectroscopy (XPS) is an experimental technique commonly employed in the surface analysis. It was widely developed in 1950s by the Kai Siegbahn's group in the Uppsala University, who was awarded the Nobel Prize in 1981 for his contribution to the photoelectron spectroscopy area. In their early days XPS was known as Electron Spectroscopy for Chemical Analysis (ESCA) because provided useful information about the chemical composition of the surface materials. In an XPS analysis the surface of the sample is irradiated with X-Ray photons of a characteristic energy like AlKα radiation (1486 eV), which is a commonly X-Ray source, after that, photoelectrons are emitted from the surface and the kinetic energy of this photoelectrons is measured, as a result of that an energy spectrum is obtained, which is usually presented as a plot of intensity (number of electrons detected per second) versus binding energy. Each element has a unique spectrum, so XPS has the ability of detect all elements except hydrogen and helium. Besides, XPS can provide information about the chemical state of the elements at the surface and the percentage present of them in an approximately depth range of 10-200 Å. In this sense X-Photoelectron Spectroscopy has been extensively used to characterize surfaces in all branches of material science.

1.1.1 Physical Basis

XPS analysis is based on the photoelectric effect which is produced when electromagnetic radiation is incised on a material, if the energy $h\nu$ of the impingement radiation exceeds the binding energy of the electron in the atom, an emission of electrons from the sample surface is generated, and these are called photoelectrons. As the name implies XPS use X-Rays to produce this effect. The photons of the incident light transfer their energy to the electrons, which absorb this energy and consequently

are ejected from core level atoms as is illustrated in **Figure 1.1**. For a better understanding of the later process, it can be explained as *three-step model* [27]. The first step happens when an electron is exited due to absorption of the incident photon, second step is when the electron travel across the sample until the surface and finally the third step is regarded as the scape of the electron from the surface to vacuum where its kinetic energy is measured.

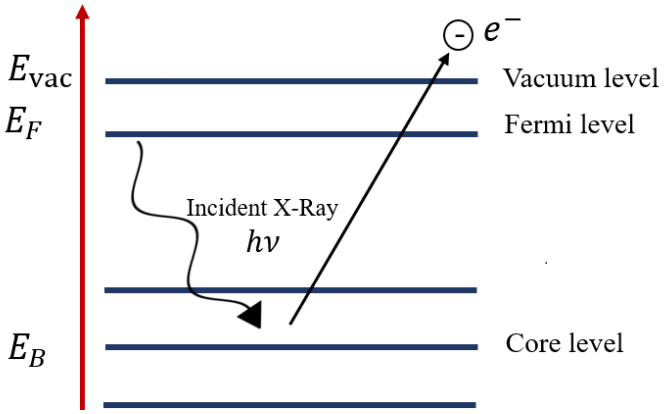

Figure 1.1. Schematic representation of photoemission process in an XPS experiment.

The kinetic energy E_k of the photoemitted electrons can be expressed as the difference between de energy of the incident radiation $h\nu$ and the sum of the binding energy of the electron in the core level and the spectrometer work function W, thus the mathematical relationship between these quantities is

$$E_k = h\nu - (E_B + W), \tag{1.1}$$

since the kinetic energy of the electron is a measurable quantity in an XPS experiment and $h\nu, W$ are known, is possible to obtain the binding energy value solving (1.1) for E_B, in such that way the expression to calculate the binding energy is as follow

$$E_B = h\nu - (E_k + W) \tag{1.2}$$

The binding energies obtained from an XPS experiment for a certain element or molecule is a distribution of the energy states in which the electrons are, in other words an XPS spectrum is a representation of the electronic structure of the material under study, in this sense phenomenon like spin-orbit coupling can be detected. This phenomenon is observed as a splitting in the energy levels that have an angular moment $l \neq 0$. These energy splitting arise from the interaction between the electron's spin and its orbital motion inside the electric field produced by the nucleus, giving a higher energy when electron's spin is parallel to the magnetic moment and lower energy when is antiparallel as is shown in the **Figure 1.2**.

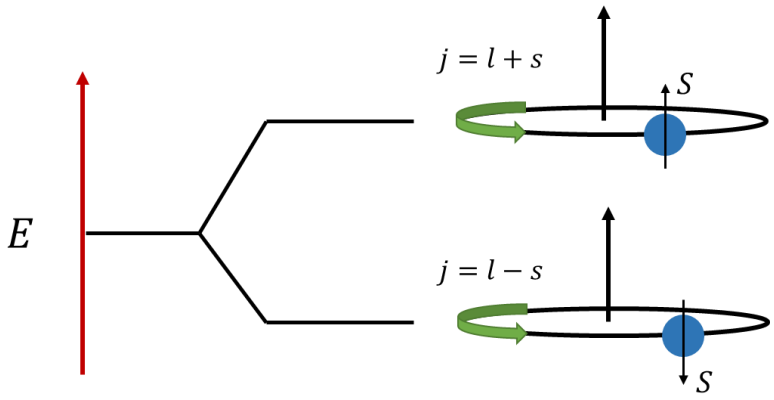

Figure 1.2 Splitting energy level with an angular $l \neq 0$ arising to the spin-orbit coupling which give a higher energy when electron's spin is parallel to the magnetic moment and lower energy when is antiparallel.

The notation employed to label each of energy states is the spectroscopists' notation [28], which is composed by three labels, the first is the principal quantum number n with positive integer values $n = 1,2,3, \ldots$, the second label is the quantum number l associated with the orbital angular moment of the electron, thus this can take the following values $l = 0,1,2, \ldots n-1$, nevertheless is usually expressed as its correspondent core sell, that is to say $0 \rightarrow s, 1 \rightarrow p, 2 \rightarrow d, 3 \rightarrow f \ldots$, and the last label is related with the spin angular moment s, this value can take 1/2 or -1/2 for fermions like electrons, this later label represent, in the spectroscopists' notation, the splitting of the energy levels due to spin–orbit coupling as we explain above, except for level s because

its angular moment is $l = 0$, the remaining levels split in two signals. Quantum numbers and their respective spectroscopists' notation are shown in **Table 1.1**.

Quantum numbers				Spectroscopists' notation
n	***l***	***s***	***j***	
1	0	1/2, -1/2	1/2	$1s_{1/2}$
2	0	1/2, -1/2	1/2	$2s_{1/2}$
2	1	1/2	1/2	$2p_{1/2}$
2	1	-1/2	3/2	$2p_{3/2}$
3	0	1/2, -1/2	1/2	$3s_{1/2}$
3	1	1/2	1/2	$3p_{1/2}$
3	1	-1/2	3/2	$3p_{3/2}$
3	2	1/2	3/2	$3d_{3/2}$
3	2	-1/2	5/2	$3d_{5/2}$

Table 1.1 The relationship between quantum numbers and spectroscopists' notation. Taken from[28].

1.1.2 XPS Line Shapes

A signal that is produced by a photoemission process is given by a Lorentzian function, the width ΔE of this function is determinate by the Heisenberg's uncertainty principle which can be expressed as follows $\Delta E \cdot \Delta\tau \geq \hbar/2$ where $\Delta\tau$ is the lifetime of the core whole state produced by the photoemission process, however in practice, both the width and the line shape are modified by the measurement process and the atomic vibrations that result in a Gaussian broadening that depends on the temperature [29], besides chemical, structural factors and electronic inhomogeneities in the surroundings of the emitting atoms can also contribute to this broadening [30]. Lorentzian and Gaussian functions have the next mathematical expressions:

$$L(E) = \left\{1 + \left(\frac{E - E_0}{\beta}\right)^2\right\}^{-1} \quad (1.3) \qquad G(E) = \exp\left\{-\ln 2\left(\frac{E - E_0}{\beta}\right)^2\right\} \quad (1.4)$$

where β correspond to half of the full width at half maximum (FWHM) and E_0 is the peak position, thus, it is common to express a XPS signal as a combination of Lorentzian and Gaussian functions, this combination is often proposed as product of these functions that is known as Voigt function [30]. Expression (1.5) is a more general line shape used to describe a XPS signal peak, because includes an asymmetric part which is used to describe loss processes like those observed in conductive materials [30].

$$f(E) = h\left\{1 + M\left(\frac{E - E_0}{\beta + \alpha(E - E_0)}\right)^2\right\}^{-1} \exp\left\{(-1 - M)\ln 2\left(\frac{E - E_0}{\beta + \alpha(E - E_0)}\right)^2\right\} \quad (1.5)$$

In the expression (1.5) are included additional parameters like the peak height h, the Lorentzian-Gaussian mixing ratio M the asymmetry index α.

1.1.3 Chemical Shift

Chemical shift is the change in binding energy between two different chemical forms of the same atom [27] and is probably the most used parameter in an XPS analysis to elucidate the chemical environment of an a certain atom, this is due to the binding energy of a core electron is usually determined by their neighbor atoms and its interaction with them. A simple way to see this phenomenon is taking only electrostatic considerations taking into account the negative charge density around the atom under study, in such way that when the electron charge density is low the binding energy tends to increase, on the contrary when the electron charge density tends to be high, the values of binding energy decrease. This happens because the effective nuclear charge in the first case increase over core electrons, due to the electrons in external shells are further away product of the interactions with neighboring atoms. A good example is the

chemical shift of ~ 7.7 eV between the binding energy of the core level C1s in $-CH_3$ and $-CF_3$ species [31], in the second molecule the carbon atom is surrounded by three fluorine atoms which have high electronegative value, thus they attract the electron density of carbon atom to itself inducing a higher binding energy in the C1s level, as it was explain some lines above. The electrostatic approach is a common explanation of the chemical shift whereas exist other phenomena like the anomalous chemical shift [32, 33] that need a broader level of theory to get a better explanation.

1.1.4 Additional spectral lines

When an X-Ray radiation is focused on a surface sample not only photoinitiation process take place, secondary process occurs and some can be detected in an XPS spectrum, some of them are explained in next pages.

Auger peaks

One of the most notable signals in an XPS spectrum is those generated by the Auger effect which happens after the photoinitiation. When a core electron is photoemitted a vacancy is generated inside the atom, this leads to a relaxation process where an electron from a higher energy level fall in the vacancy generated by the emitted photoelectron, as a consequence of this relaxation, there is a probability that an electron will be ejected, thus in this case the expelled electron is called Auger electron [28]. The nomenclature used to name this type of electrons is as follows, suppose that the photoemitted electron is expelled from a *K* shell, after that an electron from a *M* shell relax and fill the vacancy and an electron from the $M_{2,3}$ shell is ejected thus this Auger electron is named *KMM*. An Auger peak is usually the sum of several peaks that come from of the transitions that involve se same shells thus it is common label them only with the letter that represent these shells in this sense a signal that is product of Auger emissions that involve K,M and M shells is named as a Auger KMM.

The identification of different chemical environments is strongly dependent of accuracy determination of the binding energies which can be difficult especially for insulator

samples due to electrostatic charge effects which can induce a shift in the binding energy scale. In several cases, is more accurate identify the chemical states of the elements present in a surface sample employing the so called "Modified Auger Parameter" [34-37], which is a modification of the Auger Parameter proposed by Wagner [38]. Due to its definition the Modified Auger Parameter avoid uncertainties in the peak positions associated with charging effects, so a charge compensation is not indispensable. The earliest Auger Parameter was expressed as the difference between the binding energies of the principal Auger and photoelectron peaks, this is

$$\alpha = E_k(C'C''C''') - E_k(C) \quad (1)$$

where $E(C'C''C''')$ is the kinetic energy of the Auger peak that is product of the transitions between the $C'C''C'''$ core levels and $E_k(C)$ is the kinetic energy of the electron emitted from the core level C, but this expression can produce problems with negative values so a modification was made to avoid this kind of values. A simple correction is adding to the equation (4) the photon energy, is not difficult to see that the expression for the Modified Auger Parameter is the following

$$\alpha' = \alpha + h\nu = E_k(C'C''C''') + E_B(C) \quad (2)$$

where $E_k(C'C''C''')$ is the kinetic energy of the Auger electron that involve the $C'C''C'''$ levels and $E_B(C)$ is the binding energy of the electron in a core level C. The Modified Auger Parameter is used to make "Chemical States Plots" that very helpful to identify several chemical states for a given element in an accurate way without a necessity of a charging reference [39].

Satellite peaks

Other spectral lines that are characteristics of an XPS spectrum are the satellite peaks, these appear generally with lower intensity around the principal peaks, this kind of peaks can be produce due to several reasons, in this sense they are named according to the physical phenomenon that has generated them. Some of this satellites are signals

that do not give crucial information about the electronic structure of the sample, instead they can complicate the analysis of the XPS spectrum, for this reason they are considerate as a unwanted signals, for example spectrometers that do not have a monochromatic X-ray source, give spectra with satellite peaks arising from extra radiation lines that are generated together the principal emission X-ray emission, for example if a conventional AlKα radiation is used, extra photoelectron peaks associated with $\alpha_3, \alpha_4, \alpha_5, \alpha_6$ and β components can appear as can we see in the **Figure 1.2**. Nowadays this problem is solved by using a quartz crystal from which a cleaner XPS spectrum can be obtained because only AlKα component is focused on the sample. Another kind of unwanted lines are the so called "ghost peaks" which are produced when the anode used to generate the X-ray radiation has impurities, arising from contamination in a twin anode or oxidation of the anode [40], this impurities can generate X-rays photons with a different energy to the principal source, thus as a consequence of this extra signal are produced in the spectrum.

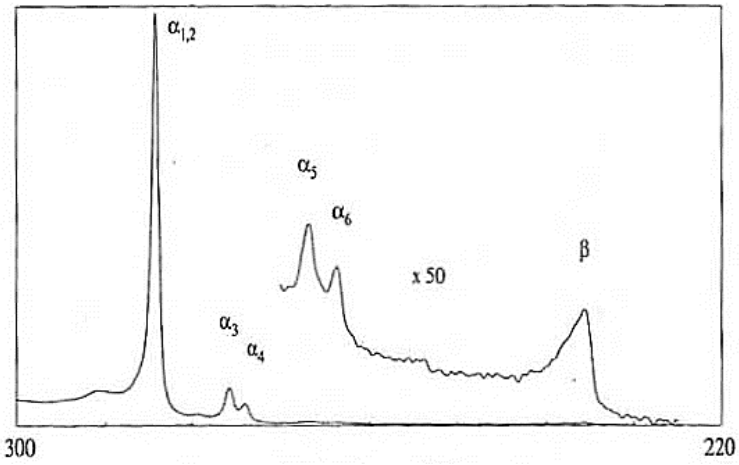

Figure 1.2 Mg x-ray satellites observed in the C1s spectrum of graphite. Taken from [40]

By other hand there are satellite peaks that offers very helpful information about the chemical state of the surface sample, for example the so called "Shake-up" satellites, this arise from the interaction of a photoelectron and an electron in the valence band, in other words the photoelectron excite a valence electron to a higher energy level in such that way the photoelectron loss part of its kinetic energy, hence appear a signal some few electron-volts above the principal core level peak in the scale of binding energy.

Shake up satellites from the 2p region of transition metals are widely used to analyze their oxide and metallic state [41-43], **Figure 1.3** its show Cu2p region where it can see the useful of sake up satellites in the identification of different cooper oxides. On the other hand, there is a shake-up satellite in the region of C1s, O1s and N1s that are used to in the analysis of valence band, structure and bonding nature of aromatic and polymers compounds [44, 45].

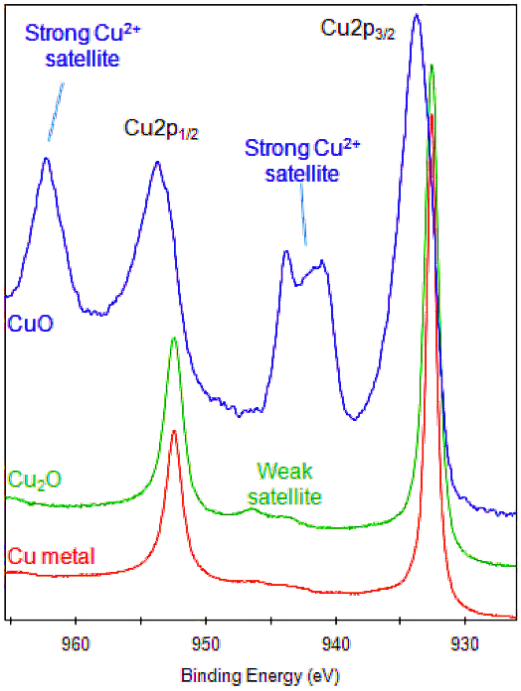

Figure 1.3 Cu 2p region for metallic cooper and cooper oxides. Metallic Cu does not exhibit satellite by other hand Cu(I) oxide present a weak satellite around 945 eV meanwhile Cu (II) Oxide has a strong satellite feature. Taken from [46]

1.2 X-Ray Photoelectron Spectroscopy applied to coordination chemistry

As we explain in the last section X-Ray Photoelectron Spectroscopy can provide good information about the chemical bonding as well the interaction with the first neighbors for a certain atom, in this sense and with an appropriate analysis could be possible deduce structural details at the surface materials from the information extracted of an XPS spectrum. The later becomes relevant due to the traditional techniques employed in the structural analysis like X-Ray Diffraction or Nuclear Magnetic Resonance give

information from bulk thus they are not a suitable to make structural studies at the surface materials. Since get structural information from an XPS analysis is not the principal application of this technique there is not a wide volume of research papers in scientific literature with this kind of studies, whereas is possible find works that reveal structural features employing X-Ray Photoelectron Spectroscopy, Ni et al studied the chemical shifts observed in the O1s and Ca2p signals of calcium carbonate polymorphs to distinguish the three phases: calcite, aragonite, and vaterite [47], their premise were, different crystals arrangements provide different chemical environments for the Ca and O atoms, as a consequence of that exhibit different binding energies . Kimata et al found correlations between the binding energies of Si2p and O1s signals of the pyrosilicate anion $Si_2O_6^{-7}$ with the different crystal structures of silica polymorphs, the authors explain that the difference in Si2p and O1s is result of SiO_4 polymerization energy among crystal structures of silica-mineral polymorphs [48].

X-Ray Photoelectron Spectroscopy also have been applied to reveal the coordination chemistry of CN and NO ligands to iron atom in transitions metal nitroprussides [49] this was achieved sensing of the redistribution density charge through the chemical sifts in the principal signals of the involved elements.

1.3 Coordination chemistry of metal carboxylates

Carboxylate anion ($RCOO^-$) is an oxygen donor ligand type with two available oxygen atoms to perform a bond, this oxygen atoms can coordinate to a metal ion in basically to forms monodentate and bidentate geometry [50]. Monodentate form is present when only one of the two available oxygen atoms is binded to a metal center, meanwhile in the bidentate form both oxygen are linked and can be appear in distinct configurations, that is why there is a wide range of geometries in which carboxylate ligand can linked, **Figure 1.4** shows the coordination modes that are typically encountered in metal carboxylates; **a-c** account for the traditional modes: monodentate, bridging bidentate and chelating, while **d-h** represent other alternatives including the ionic behavior.

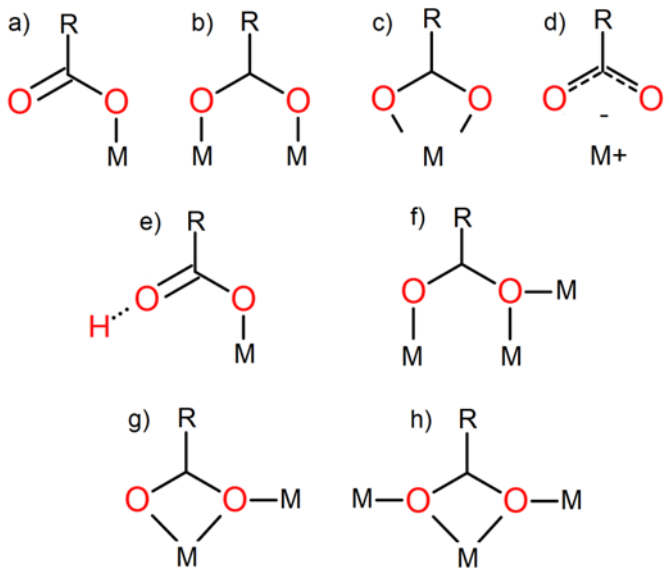

Figure 1.4 Binding modes for metal carboxylates: a) Monodentate, b) Bridging Bidentate, c) Chelating, d) Ionic, e) Pseudo Bridging Bidentate, f) Bridging ($\mu_3\eta^1\eta^2$Mode), g) Chelating Bridging and h) Chelating Bridging ($\mu_3\eta^1\eta^2\eta^1$Mode).

The wide range of geometries that present the carboxylate ligand is result of the two electrons lone pairs in each oxygen atom which are available to bind with a metal center. The most common binding modes are those that involve *syn* lone pairs like monodentate, chelating, and bidentate bridging due to present greater basicity than *anti* lone pairs [51].

1.4 Techniques and methods for the identification of metal carboxylates coordination modes

1.4.1 Nuclear magnetic resonance (NMR)

Some spectroscopic techniques have been used to the distinction of carboxylates coordination modes especially in the cases where no structural information is available or when the experimental conditions are not suitable to employ techniques like X-Ray Diffraction. In science literature there are studies that employ Nuclear Magnetic Resonance (NMR), to elucidate the coordination modes of metal carboxylates [19, 20], this studies associate the ^{13}C chemical shifts of carbon atoms in the carboxylate group

with the different binding modes of carboxylate complexes, on the basis that the shielding over the carbon atoms involved in the carboxylate group varies according to the binding geometry, thus this variation it could be observed when comparing different coordinations. Ye et al study zinc-carboxylate complexes by ^{13}C CP/MAS NMR technique and found that the values of chemical shifts of different coordination modes follow the next relationship: chelating mode (184 ppm) > bidentate bridge (180 ppm) > monodentate bridge (176 ppm) [20], in other similar study Lin et al made a research of acetato porphyrinato metal complexes employing ^{13}C NMR of the methyl and carbonyl carbons, they conclude that the ^{13}C methyl and carbonyl chemical shifts have values of 20.5 ± 0.2 and 168.2 ± 1.7 ppm respectively, for monodentate geometry meanwhile the chelating bidentate mode have chemical shifts values of 18.0 ± 0.7 and 175.2 ±1.6 ppm for methyl and carbonyl respectively [19].

1.4.2 Infra-Red Spectroscopy (IR)

Raman Spectroscopy [21, 22] and Infra-Red Spectroscopy (IR) [23] also have been employed to identify the coordination mode of metal carboxylates. Both Raman and IR spectroscopies have a similar methodology which is based in the magnitude of the separation between the frequency of asymmetric $V_{as}(COO^-)$ and symmetric $V_{sym}(COO^-)$ carboxylate vibration, $\Delta = V_{as}-V_{sym}$, as indicative of coordination geometry, whereas the methodology that use Infra-Red Spectroscopy is widely more employed in fact the research paper wrote by Deacon et al in which a detailed analysis by means IR Spectroscopy was made [23], have been cited more than 4000 times at the moment that this thesis has been written. In the mentioned work the authors propose that monodentate complexes present Δ values greater than ionic complexes, this arise from fact that in monodentate arrangement the oxygen atoms are not equal, in other words they have different bond order which lead to an increase in the Δ value on the other hand chelating and bridging complexes have Δ similar values but lower than ionic [23] thus they conclude that the following relationship is valid.

$$\Delta(\text{Chelating}) \cong \Delta(\text{Bridging}) < \Delta(\text{ionic}) < \Delta(\text{monodentate}) \qquad (1.1)$$

However, this relationship has to be carefully applied especially when very low Δ values appear since it could be indicating a combination of chelating and bridging [23] and when hydrogen bonds are present since in this situation it might not be possible distinguish between bridging and pseudo bridging bidentate.

CHAPTER II: EXPERIMENTAL SECTION

2.1 Materials and Equipment

To elucidate the coordination mode in transition metal carboxylates, we choose model compounds that were stable under ultra-high vacuum conditions and have the least amount of carbon and oxygen atoms with different environments to those involved in a metal carboxylate, this in order to obtain cleaner signals in the XPS spectra. After a thorough search in the literature and the structural databases PDF-4 Organics 2018 and The Cambridge Crystallographic Data Centre (CCDC) we conclude that metal acetates are a suitable model compounds due to these satisfy the required conditions. In the first approach we consider studying only the monodentate, bridging bidentate and chelating geometries, due to these arrangements are the most common, but in order to achieve a wide analysis, we consider additional bidentate geometries, the ionic interaction and the monodentate geometry with hydrogen bond interaction (pseudo bridging bidentate). The model compounds studied here are the following: Bis Thiourea Zinc Acetate (BTZA) $Zn(NH_2CSNH_2)_2(CH_3COO)_2$, Mercury(II) acetate $Hg(CH_3COO)$, Copper (II) acetate monohydrate $Cu(CH_3COO)_2(H_2O)$, Zinc acetate $Zn(CH_3COO)_2$, Zinc acetate dihydrate $Zn(CH_3COO)_2 2(H_2O)_2$, Copper Acetate Diammine $Cu(CH_3COO)_2{\cdot}2NH_3$, Cadmium acetate dihydrate $Cd(CH_3COO)_22(H_2O)$, Lead(II) acetate trihydrate $Pb(CH_3COO)_23(H_2O)$, Copper(II) acetate $Cu(CH_3COO)_2$, Manganese(II) acetate $Mn(CH_3COO)_2$, Sodium acetate NaCH3COO, Lithium acetate dihydrate $Li(CH_3COO)_22(H_2O)$, Nickel(II) acetate tetrahydrate $Ni(CH_3CO_2)_2{\cdot}4(H_2O)$, Cobalt (II) acetate tetrahydrate $Co(CH_3CO_2)_2{\cdot}4(H_2O)$ and Magnesium acetate tetrahydrate $Mg(CH_3CO_2)_2{\cdot}4(H_2O)$.

All geometries corresponding to each model compound are summarized in **Table 2.1**. Each coordination mode of the mentioned compounds was confirmed by identifying their crystal structures through X-Ray Powder Diffraction using the PDF-4 Organics 2018 database. The X-ray powder diffraction (XRD) patterns were recorded at room conditions using a D8 Eco Advance diffractometer (from Bruker) and CuKα radiation.

	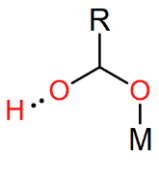	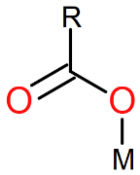	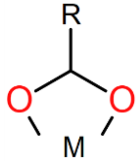	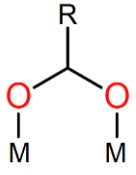	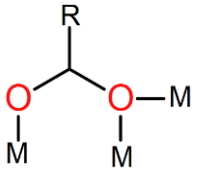	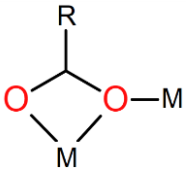	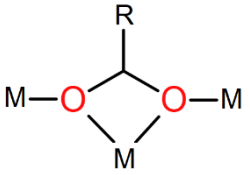	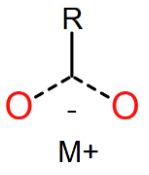
Zn		BTZA	ZnAc $2H_2O$	Zn Ac				
Cu			Cu Ac NH_2	Cu Ac H_2O	Cu Ac			
Cd						Cd Ac $2H_2O$		
Mn					Mn Ac			
Co	CoAc $4H_2O$							
Hg		Hg Ac						
Ni	NiAc $4H_2O$							
Pb							Pb Ac $3H_2O$	
Na								Na Ac
Li								Li Ac $2H_2O$
Mg	MgAc $4H_2O$							

Table 2.1 Model compounds studied here and their respective binding mode. From left to right: Pseudo Bridging Bidentate, Monodentate, Chelating, Bridging Bidentate, Bridging ($\mu_3\eta^1\eta^2$Mode), Chelating Bridging, Chelating Bridging ($\mu_3\eta^1\eta^2\eta^1$Mode) and Ionic.

Zinc acetate Zn $(CH_3COO)_2$ and Copper (II) acetate $(CH_3COO)_2$ were obtained from a thermal treatment applied to their correspondent hydrated compounds, Zn $(CH_3\ COO)_2\ 2(H_2\ O)_2$ and Cu $(CH_3COO)_2(H_2\ O)$. As the thermographs show in the **Figure 2.1** the anhydrous phase of Zn $(CH_3\ COO)_2\ 2(H_2\ O)_2$ was obtained around of 80º degrees centigrade meanwhile the anhydrous phase of Cu $(CH_3COO)_2(H_2\ O)$ was obtained around 108º degrees centigrade. After the thermal treatment was applied over these compounds, their structure and consequently their coordination mode was verify again using X-Ray Powder Diffraction. Thermogravimetric analyses were carried out in dynamic high-resolution mode with a TGA Q5000 equipment at 10 °C/min ratio in a nitrogen atmosphere.

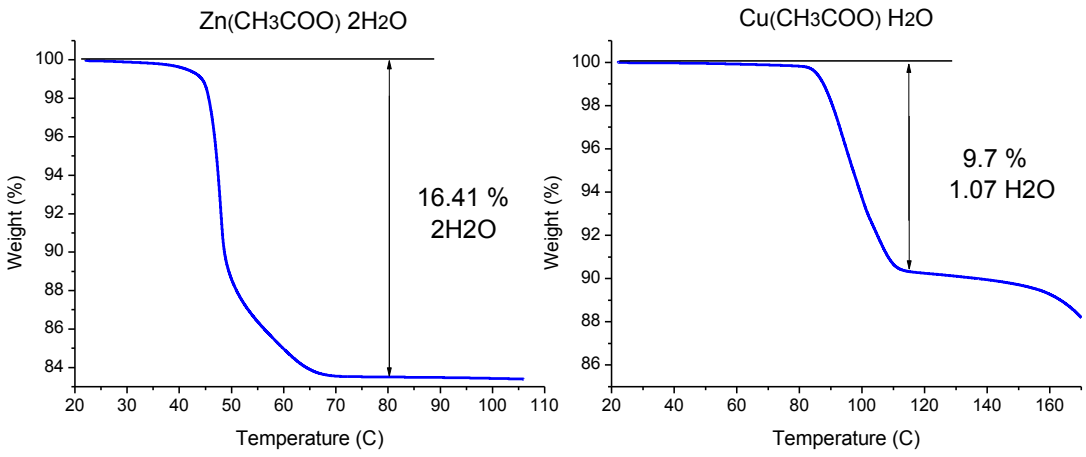

Figure 2.1 Thermal decompositions diagrams of Zinc Acetate dihydrated Zn $(CH_3COO)_2\ 2H_2O$ (left) and Cu $(CH_3COO)\ H_2O$ (right). Anhydrous phase of Zn $(CH_3COO)_2\ 2(H_2O)$ was obtained around of 80º Celsius degrees meanwhile the anhydrous phase of Cu $(CH_3COO)_2\ (H_2O)$ was obtained around 108º Celsius degrees.

Synthesis of (BTZA) and Cu $(CH_3COO)_2 \cdot 2NH_3$

Only BTZA and Copper Acetate Diammine were synthesized, the remaining model compounds were provided from Sigma Aldrich and measured directly without further purification.

Bis Thiourea Zinc Acetate (BTZA)

Bisthiourea Zinc Acetate was prepared by a rout of synthesis described by Kadam et al [52]. 100 mg of zinc acetate dihydrate was dissolved in 5 ml of methanol under stirring. At the same time, 69.3 mg of thiourea was dissolved in 5 ml methanol under stirring. The dissolved thiourea was added drop-wise to the dissolved zinc acetate in methanol solution. Under stirring, white precipitate was formed after methanol evaporation.

Copper Acetate Diammine $Cu(CH_3COO)_2 \cdot 2NH_3$

Copper Acetate Diammine was prepared in a similar way of the method described by Euler et al [53]. A nearly saturated solution of distilled water and copper acetate monohydrate was prepared and heated up to 85 °C then a 6 M solution of ammonium hydroxide was adding by dropwise. After the reaction mixture is cooled the resulting compound was washed several times with acetone.

2.2 XPS measurements

All XPS measurements were performed using a Thermo Scientific K-Alpha X-ray photoelectron spectrometer with hemispherical analyzer and a typically monochromatic Alkα X-ray source (1486.6 eV) in the Constant Analyzer Energy (CAE) mode, the base pressure of analyzer chamber was $1 \times 10{-}9$ mBar. The charge corrections of all spectra were referenced to the position of the C1s adventitious peak at 284.8 eV. Survey scans were recorded using 400 μm spot size and fixed pass energy of 200 eV, whereas high resolutions scans were collected at 20 eV analyzer pass energy in order to obtain a high resolution in the collected spectra. The elemental analysis does not reveal contamination in the studied compounds beyond to the adventitious contamination which corresponds to hydrocarbon species present in all air exposed materials, by other hand the quantification analysis was accordingly to the stoichiometric relationships of the model compounds. The peak fitting was carried out employing a mixed Gaussian-Lorentzian product function with a 30 % L/G ratio and a Shirley type background.

CHAPTER III: RESULTS AND DISCUSSION

3.1 Experimental Characterization

3.1.1 Infra-Red Spectroscopy (IR)

Besides the X-Ray Powder Diffraction characterization an Infra-Red analysis was performed, this in order to identify the corresponding bands associated with the asymmetric V_{as} (COO-) and symmetric V_{sym} (COO-) stretching carboxylate vibrations and consequently calculate the difference between their positions $\Delta = V_{as}-V_{sym}$, this so as to perform a comparison among the methodology used to determine the coordination mode proposed by Deacon et al and the results obtained by our XPS analysis. It is important to mention that the relationship (1.1) proposed by Deacon et al [23] is not a general rule, because could be fail in some cases, but is very useful specially when no structural data is available. In **Annex A** we show the IR spectrum of each model compound, organized in the different coordination modes, in the region associated with symmetric and asymmetric stretching vibrations of the carboxylate group and their respective position in the spectrum. With the information obtained from the data in **Annex A** we build the **Table 3.1** in which we present the values of $\Delta = V_{as}-V_{sym}$ for each compound and their respective binding mode.

Pseudo Bridging Bidentate mode is a remarkable geometry because as its name implies is a pseudo bridging arrangement due to both oxygen atoms in the carboxylate anion are involved in bonds with other atoms, but only one of them have a covalent bond with a metal atom, meanwhile the reaming oxygen have a hydrogen bond which is product of the interaction with a molecule water present in the structure as in shown the **Figure 3.1**, in other words this kind of geometries are a monodentate carboxylate with an additional interaction, in this case a hydrogen bond.

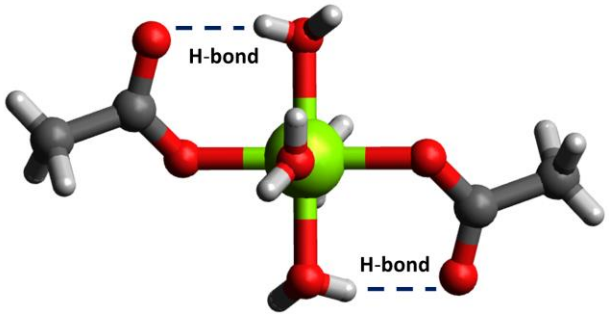

Figure 3.1 The so called Pseudo Bridging Bidentate. This binding mode is a monodentate geometry with an additional interaction, a hydrogen bond.

The later triggers that the differences among the energies associate with the symmetric and asymmetric COO vibration be small. As a result of that the parameter Δ for this binding mode have values, around 100 cm^{-1} which is low in comparison with the ionic values which are around the 155 cm^{-1}. On the other hand accordingly to the expression (1.1) the MAc $4H_2O$ with M= Ni, Co, Mg compounds could be classified as a pure bridging or chelating compounds, but as we saw this cannot be accurate specially when hydrogen bonds are present, thus at this point, in order to have a better image of the binding geometry a structural data is needed, but as we treat in next sections we can use information obtained from an high resolution XPS spectra to solve this problem.

Binding Mode	**Compound**	**V_{as} cm^{-1}**	**V_{sym} cm^{-1}**	**Δ cm^{-1}**
Pseudo Bridging Bidentate	Ni Ac $4H_2O$	1515	1416	99
	Co Ac $4H_2O$	1519	1415	104
	Mg Ac $4H_2O$	1531	1421	110
Monodentate	BTZA	1577	1395	182
	Hg Ac	1566	1362	204
Chelating	Zn Ac $2H_2O$	1553	1434	119
	Cu Ac NH_2	1565	1399	166
Bridging Bidentate	Cu Ac H_2O	1600	1418	182
	Zn Ac	1540	1447	93
Bridging ($\mu_3\eta^1\eta^2$Mode)	Cu Ac	1588	1425	163
	Mn Ac	1568	1380	188
Chelating Bridging	Cd Ac $2H_2O$	1529	1444	85
Chelating Bridging ($\mu_3\eta^1\eta^2\eta^1$Mode)	Pb Ac $3H_2O$	1526	1387	139
Ionic	Na Ac	1557	1409	148
	Li Ac $2H_2O$	1593	1432	161

Table 2.1 Infrared frequencies (cm^{-1}) of symmetric Vas (COO-) and symmetric Vsym (COO-) bans of different binding modes in transition metal carboxylates.

In the case of a pure monodentate geometry as the BTZA and Hg Ac compounds the Δ parameter presents high values, 182 cm^{-1} and 204 cm^{-1} respectively which is expected for this binding mode due different bond orders of C-O and C=O in the carboxylate group, this confirm the difference between a pure monodentate compound and a monodentate with hydrogen bond interaction commonly named Pseudo Bridging Bidentate mode.

For the Chelating compounds as the expression (1) suggest should be have Δ values below 155 cm^{-1}, it is clear that Zn Ac $2H_2O$ with Δ = 119 cm^{-1} is according to the proposed relationship but the case of Cu Ac NH_3 is different, because this compound has a Δ = 166 cm^{-1} which is slightly above of the ionic parameter, these experimental results can be explained as follows: the crystal structure reported in the Cambridge Crystallographic Data Base show that there is a noteworthy difference among the C-O bond lengths in the carboxylate groups belonging to each compound, the above is shown clearly in **Figure 3.2** in which it can see that C-O bond lengths for Zn Ac $2H_2O$ are very similar, with a difference only about 0.006 Å, meanwhile C-O bond lengths in Cu Ac NH_3 differ in 0.036 Å, these differences are directly reflected in the positions of their asymmetric V_{as} (COO-) and symmetric V_{sym} (COO-) carboxylate vibrations in a IR spectrum, in such that way due to Zn Ac $2H_2O$ is more symmetric in its geometry, thus present values according with a pure chelating mode by other hand Cu Ac NH_3 "tend to a monodentate geometry" due to its asymmetric geometry reflected in their C-O bond lengths, but this difference is not larger like in a monodentate compound, for this reason Cu Ac NH_3 present a high Δ values but without reaching values belonging to pure monodentate compounds.

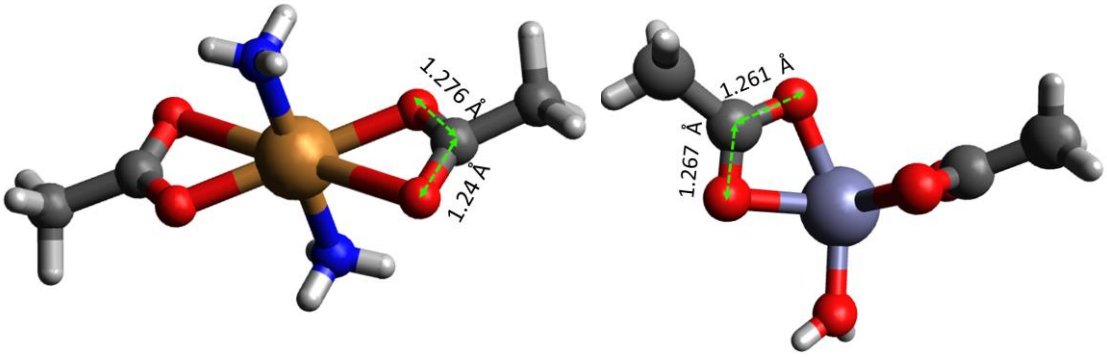

Figure 3.2 C-O bond lengths in the carboxylate group for Cu Ac NH_3 (left) and Zn Ac $2H_2O$ (right), both are chelating compounds but Cu Ac NH_3 present a asymmetry in its carboxylate geometry.

Zn Ac is the anhydrous phase of Zn Ac $2H_2O$ and is a Bridging Bidentate Compound which present a $\Delta = 93\ cm^{-1}$ thus is according to the expression (1.1), by other hand the remaining Bridging Bidentate Compound Cu Ac H_2O, is an exception of the rule because has a $\Delta = 188\ cm^{-1}$ and in accordance with its reported structural data has pure symmetric Bridging Bidentate geometry.

As can we see, the determination of the binding geometry employing the methodology based in the value of $\Delta = V_{as}-V_{sym}$ have to be carefully carried out in order to obtain reliable information which can be supported with additional characterization techniques.

3.1.2 X-Ray Photoelectron Spectroscopy (XPS)

3.1.2.1 C1s Region

XPS spectra of C1s of different metal carboxylates geometries were carried out in order to inspect how the C1s binding energies of the carbon atoms in the model compounds are modified in dependence of the binding mode. Fig. 2 Show high-resolution C1s spectra of different coordination modes: Ionic, Monodentate, Bridging Bidentate and Chelating. In C1s region, it is common to find signals of adventitious carbon contamination which are observed in air-exposed materials [54] for this reason; it is quite important to perform a suitable analysis to be able to distinguish this kind of signals from those that belong to the studied materials. In our analysis of the C1s region

of all model compounds, the components of carbon contamination identified were peaks with binding energies values around 284.8 eV , 286.4 ± 0.3 eV, 287.7 ± 0.2 and 290 ± 0.2 , which are related to saturated carbon C-C and C-H [54] , ether or epoxy groups C-O [31, 55, 56] , carbonyl group C=O [31, 57, 58] and carbonate group [31] respectively. In only one case, it was detected a small peak below the hydrocarbon peak at 283.8 eV, which is according to literature it could be attributed to a metal carbide species as a possible consequence of the X-ray beam damage.

The most prominent peaks at 285.4±0.1 eV and 288.9±0.2 eV were assigned to the carbon signals of methyl and carboxylate group respectively, these functional groups belong to model compounds studied here. After the fitting was carried, it could be noticed that the stoichiometric ratios between CH3 and COO species was approximately 1:1 which is in a good agreement with the theoretical quantification, the latter suggests that a good peak fitting was done. It is important to mention that an exact ratio of 1:1 between the CH3 and COO species is hard to achieve due to the presence of small quantities carbon contamination species that could be in similar binding energies and that could be contributing at the time of quantification.

Binding energy associated with the core level C1s correspondent to methyl group, of all studied compounds, does not show significant variations (285.4±0.1), just as expected because of lower interaction with the carboxylate group, in other words this means that all these carbon atoms are chemically equivalent, whereas the signal C1s of the carbon atom belonging to the carboxylate group, which appear at higher values of binding energies, present a slightly but notable change in the positions in dependence of their corresponding binding geometries, the latter is reflected in a wider range of variation around 288.8±0.2 eV , this is a consequence of the direct influence of oxygen atoms involved in the coordination mode. These variation can be explained as follows, the electronic charge around the carbon atom varies according to the type bond of the carboxylate oxygen atoms with the metal center, thus as a result of that, as it is possible to see in the **Figure 3.3 a-d**, there is a shift in the position of C1s peak associated with COO species. A general view of the chemical shifts observed from the data collected corresponding to different coordination modes is presented in **Figure 3.4** where the C1s binding energy intervals for all the coordination modes studied here, are plotted. In this

graph it can be noted that geometries like monodentate and ionic tend to lower binding energies than chelating, bridging bidentate and pseudo bridging bidentate geometries, this difference between these two groups, is principally due to the nature of interaction type among carboxylate anion and the metal atom. In the first case, ionic interaction has a delocalized negative charge over the two oxygen atoms that make up the carboxylate anion, because of that, more negative charge is present around the carbon atom. In the monodentate geometry a similar environment is present because there is still negative charge shared with the oxygen atom in the carbonyl group. On the other hand in the chelating and bridging geometries, both oxygen share negative charge with the metal center, leaving the carbon atom less shielding, therefore the electrostatic potential is different, leading to a chemical shift at higher binding energies of C1s level.

Despite there is an observable difference in the positions of the C1s peak related with COO species, the interval where all signals appear, is quite narrow to establish a good parameter to distinguish between the different coordination modes, and as can we see in the **Figure 3.4** some of the binding energy intervals .

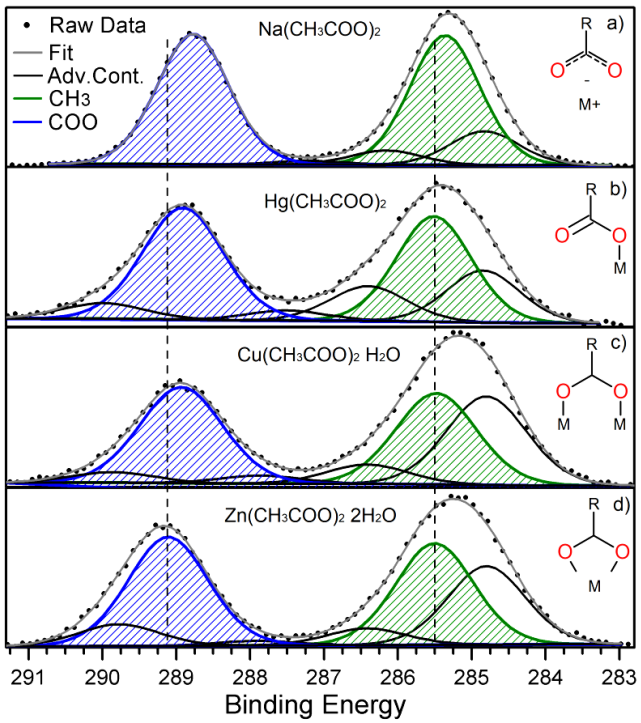

Figure 3.3 C1s peak of metal acetates with different geometries: a) Ionic, b) Pseudo Bridging Bidentate, c) Bidentate and d) Chelating. Peak fitting show the assignment of CH3 and COO species, the remaining peaks (black line) were assigned to adventitious contamination species. C1s peak of COO group appear in different positions due to distinct chemical environments.

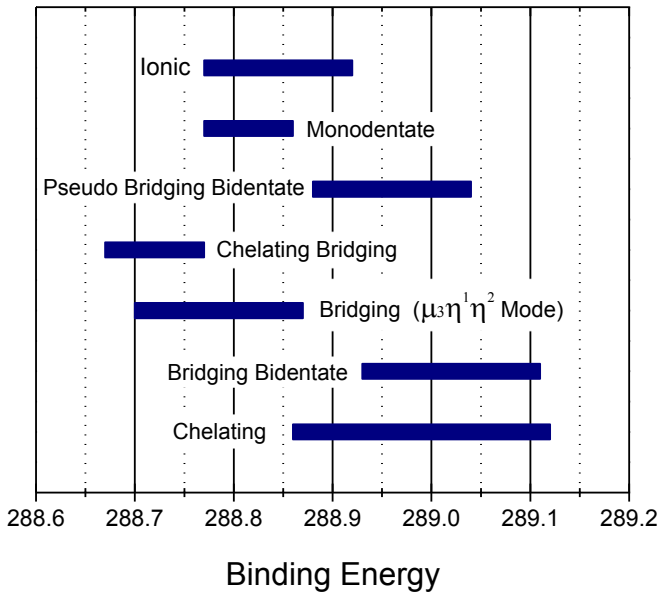

Figure 3.4 C1s binding energy ranges for various coordination modes. Monodentate and ionic geometries tend to lower binding energies than Chelating, Bridging Bidentate and Pseudo Bridging Bidentate geometries.

3.2 O1s Region

XPS spectra of O1s signal of different metal carboxylates geometries were carried out. Since all materials examined were exposed to air, all of them present the common adventitious contamination, as can we see in the C1s region. Several of the species that make up this contamination have functional groups that contain oxygen atoms, thus the latter can be detected in the signals O1s in addition to other species like, oxides or the carboxylate oxygen atoms that belong to the model compounds. Whereas, it is complex identify this contamination species because some of them have low atomic percentages compared with the most prominent peaks, furthermore present binding energies with values in the same region of the carboxylate or water oxygens studied here. On other hand species containing oxygens with higher binding energies (533.4 ±0.4) like ether or ester [31] and lower binding energies like metal oxides (530 ±0.5) [41, 59, 60] could be identified in our spectra but with a low atomic percentage.

An extensive examination of the O1s core level reveals important characteristics that lead to an identification of different coordination modes. First, as can we see in the

Figure 3.5 there is a chemical shift in the position of COO O1s signal for different binding modes, in a similar way from that found in the C1s region, but with a larger separation between the peaks, besides this, chemical shifts confirm the previously observed in the C1s region, this is, geometries like chelating and bridging bidentate have higher binding energies than ionic, due to oxygen atoms in ionic interaction, are more shielding than chelating and bridging bidentate geometries, as we explain previously. Additionally, as Fig. 5 show, O1s provide more certainty about the number of signals and the binding energies that present the different coordination modes. Ionic interaction presents only one peak located at binding energies values around 531.5-531.6 eV and they are typically conformed by alkali metals. Monodentate geometry presents two peaks, because of the different chemical environment of the two oxygens in the structure, one of them is associated with C=O bond and other is associated with C-O-Metal bond, with a approximately stoichiometric ratio 1:1. The first signal appears at 531.5-531.6 eV while the second appears at higher binding energies in the interval 532.2 ± 0.1. Pseudo Bridging Bidentate is a special case of monodentate geometry with hydrogen bond interaction this present one peak but broader than ionic, as a consequence of the overlapping of two signals, coming from the two oxygen in C-O-Metal an C-O--H bond. Besides this it is necessary to take in count the presence of the molecules waters in the structure and the ratio between them and the carboxylate oxygen atoms. Since all Pseudo Bridging Bidentate model compounds studied here are isomorphous, with a generic formula M (CH3COO) 2·4(H2O) where M = Co, Ni, Mg, a very similar fitting was obtained in the three cases. The O1s peak for this geometry is conformed by two peaks in an approximately 1:1 stoichiometric ratio, one peak corresponds to the water molecules in the structure and the remaining is associated with carboxylate oxygen atoms. As a result of the latter, it was concluded that this carboxylate oxygen atoms have similar chemical environments, in other words, present similar binding energies in such way that appear as one peak at 531.6 eV. It is important mentioned that a fit with three components, which can distinguish two types of oxygen atoms in the in the carboxylate group, was discarded because there is no possibility to acquire a good fitting, with a reasonable atomic ratio that corresponds to the chemical formula M (CH3COO) 2·4(H2O). The remaining geometries, Chelating and Bridging

Bidentate exhibit similar characteristics, both have only one peak associated with the carboxylate group, showing the chemical equivalence of their oxygen atoms just as expected. In these geometries, the electron density over the oxygen atoms in the carboxylate group tend to be closer of the metal center than the oxygen atoms, in other words, they are less shielding, thus tend to have high binding energies than other geometries, 532-532.1 eV for chelating binding mode and 532 ± 0.1 eV for Bridging Bidentate.

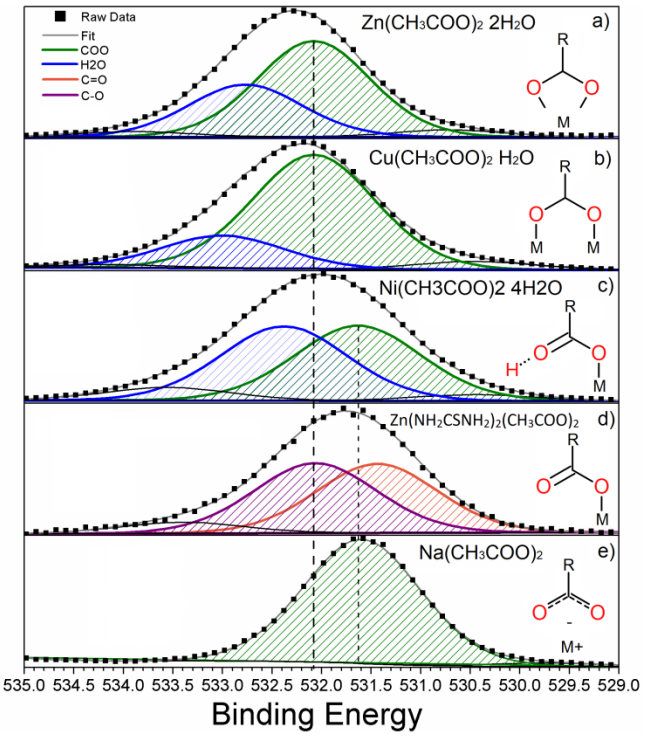

Figure 3.5 O1s peak of metal acetates with different geometries: a) Chelating, b) Bridging Bidentate, c) Pseudo Bridging Bidentate, d) Monodentate and e) Ionic. Peak fitting show different chemical shifts for distinct coordination modes. Only in the Monodentate geometry is possible distinguish two types of oxygen atoms C-O-M and C=O.

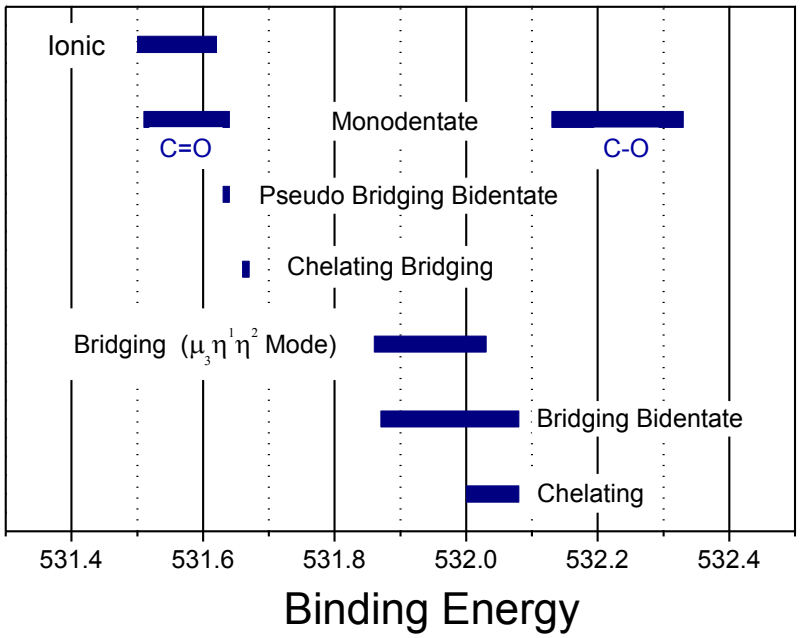

Figure 3.6 O1s binding energy ranges for various coordination modes. Ionic and Pseudo Bridging Bidentate geometries present lower binding energies than chelating and bridging Bidentate. Monodentate geometry is characterized by the presence of two signals associated with oxygen atoms in C-O-M and C=O bonds.

CONCLUSIONS

We have discussed the possibility of employ X-Ray photoelectron spectroscopy as a tool to identify the coordination geometry of metal carboxylates. We found that C1s and O1s signals, coming from oxygen and carbon atoms belonging to the carboxylate group, are sensitive to different coordination modes. This sensitivity is observed in the chemical shift of the C1s and O1s positions. The C1s chemical shifts are not large enough to establish a good methodology that leads to diagnose the coordination mode. On the other hand O1s signal exhibit larger chemical shifts that lead to the identification of different coordination geometries. We found that Ionic interaction present only one peak located at binding energies values around 531.5-531.6 eV, Monodentate geometry present two peaks, due to different chemical environment of the two oxygen atoms, one of them is associated with C=O bond and other is associated with C-O-Metal bond, at 531.5-531.6 eV and 532.2 ± 0.1 respectively, Pseudo Bridging Bidentate presents one peak at 531.6 eV as a result of overlapping of the O1s peaks that appear a very similar binding energy values and correspond to the oxygen atoms in C-O-Metal and C=O--H bonds, the remaining geometries, Chelating and Bridging Bidentate show one peak that tend to have high binding energies than other geometries, 532-532.1 eV and 532 ± 0.1 eV respectively.

ANEX A: IR SPECTRA OF MODEL COMPOUNDS CLASSIFIED BY BINDING MODE

Pseudo Bridging Bidentate Mode

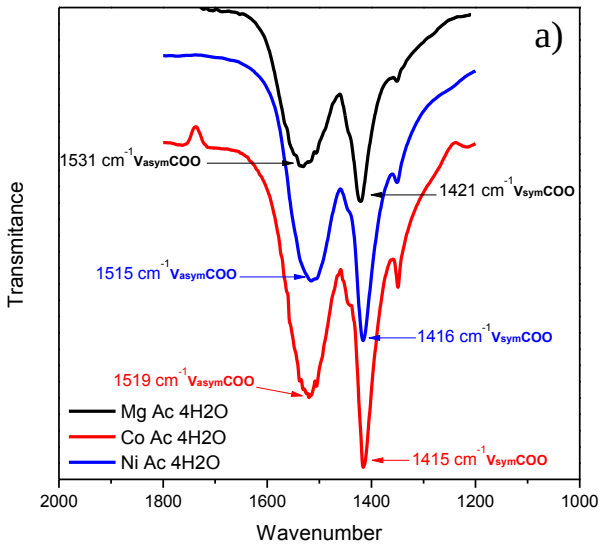

Monodentate Mode

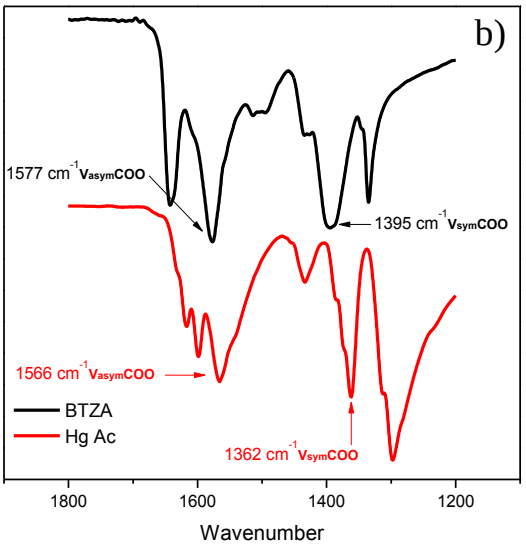

Chelating Mode

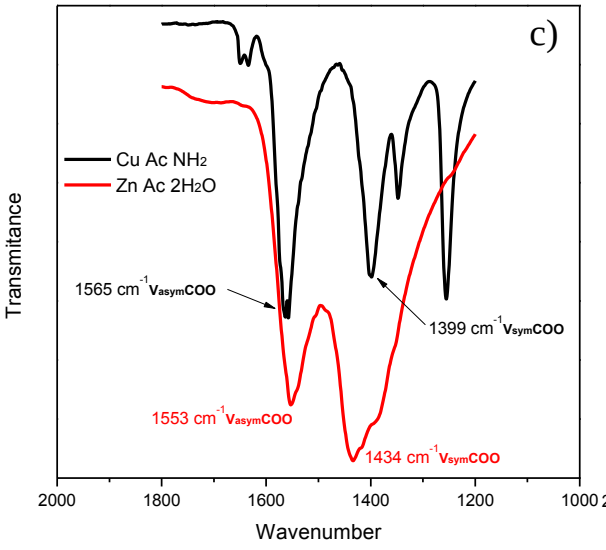

Bridging Mode

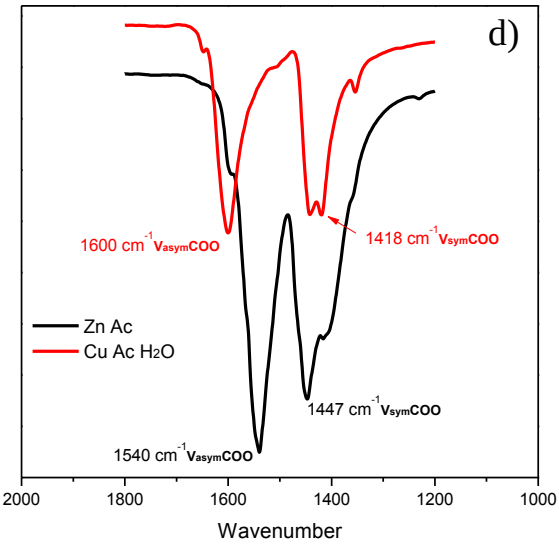

Bridging ($\mu_3\eta^1\eta^2$Mode)

Chelating Bridging

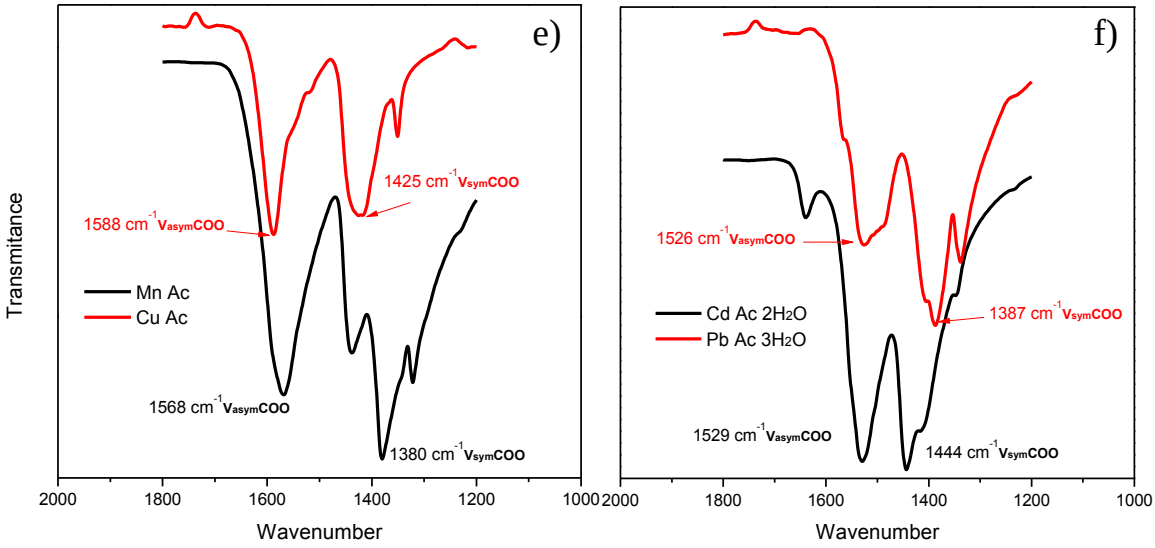

Ionic

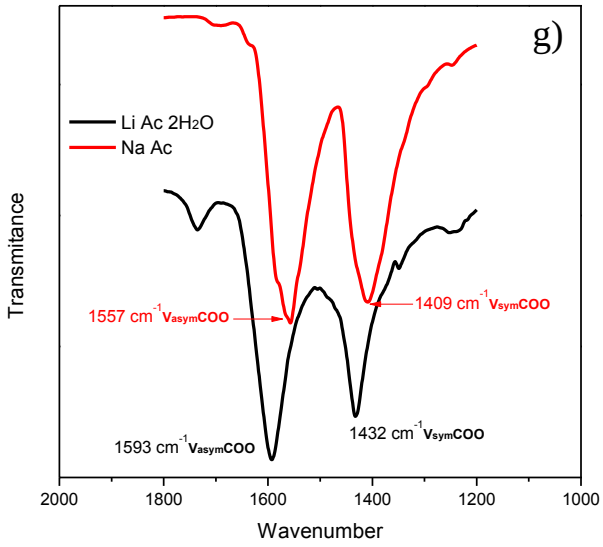

ANEX B: C1s AND O1s BINDING ENERGIES OF THE MODEL COMPOUNDS

Binding Mode	**Compound**	**Binding Energy CH3 C1s**	**Binding Energy COO C1s**	**Binding Energy COO O1s**
Chelating	$Zn(CH_3COO)_2 2(H_2O)_2$	285.5	289.12	532.08
	Cu (CH3COO)2 2NH3	285.51	288.86	532.00
Bridging Bidentate	Cu(CH3COO)2(H_2O)	285.48	288.93	532.08
	Zn(CH3COO)2	285.49	289.11	531.87
Bridging ($\boldsymbol{\mu_3\eta^1\eta^2}$Mode)	Mn(CH3COO)2	285.30	288.70	531.86
	Cu(CH3COO)2	285.43	288.87	532.03
Chelating Bridging ($\boldsymbol{\mu_3\eta^1\eta^2\eta^1}$Mode)	Pb(CH3COO)23(H_2O)	285.34	288.67	531.66
Chelating Bridging	Cd(CH3COO)22(H_2O)	285.37	288.77	531.67
Pseudo Bridging Bidentate	Mg(CH3CO2)24(H2O)	285.47	289.04	531.64
	Ni(CH3CO2)24(H2O)	285.53	288.95	531.63
	Co(CH3CO2)24(H2O)	285.32	288.88	531.63
Monodentate	Zn(NH2CSNH2)2(CH3COO)2	285.49	288.77	**O1:** 531.51 **O2:** 532.13
	Hg(CH3COO)2	285.46	288.86	**O1:** 531.64 **O2:** 532.33
Ionic	NaCH3COO	285.36	288.77	531.62
	Li(CH3COO)22($H_2O)_2$	285.33	288.92	531.50

Table B.1 C1s and O1s binding energies for various coordination modes. Ionic and Pseudo Bridging Bidentate geometries present lower binding energies than chelating and bridging Bidentate. In O1s region Monodentate geometry is characterized by the presence of two signals associated with oxygen atoms in C-O-M and C=O bond

ANEX C: FITTIGN OF C1s AND O1s REGIONS OF MODEL COMPOUNDS

C1s Region

Pseudo Bridging Bidentate Mode

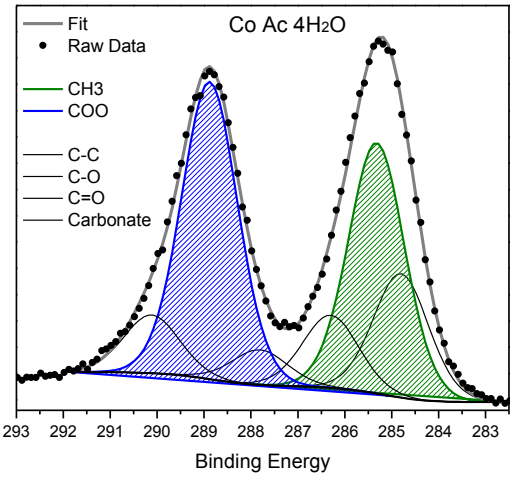

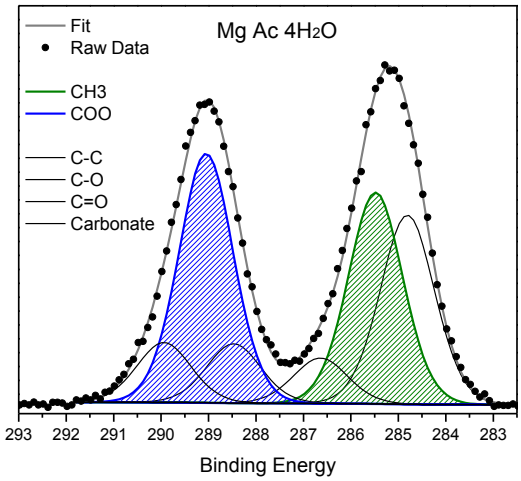

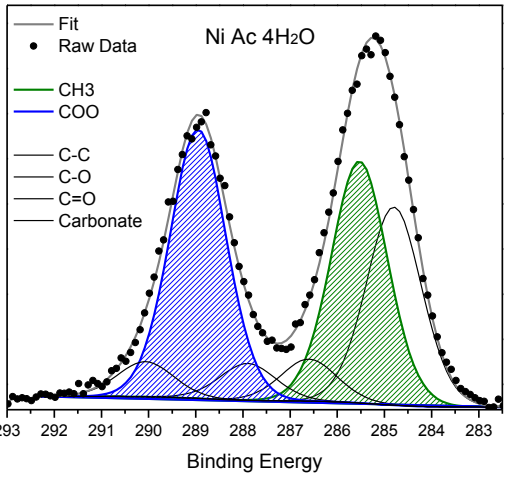

Monodentate Mode

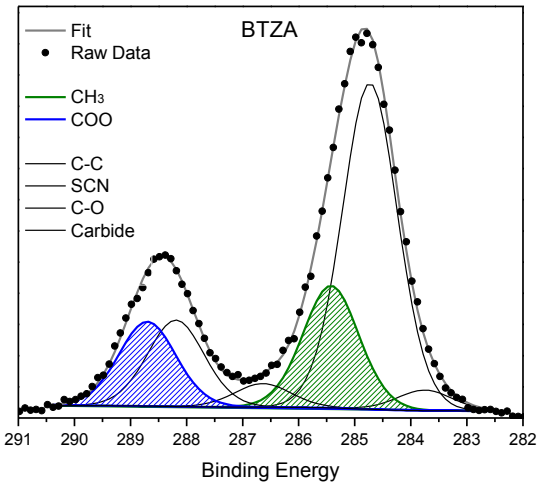

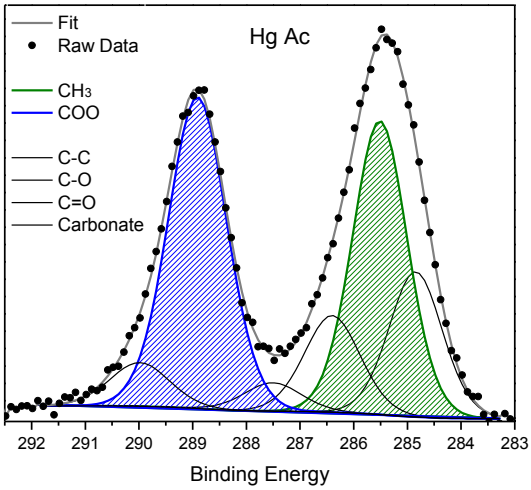

Chelating Mode

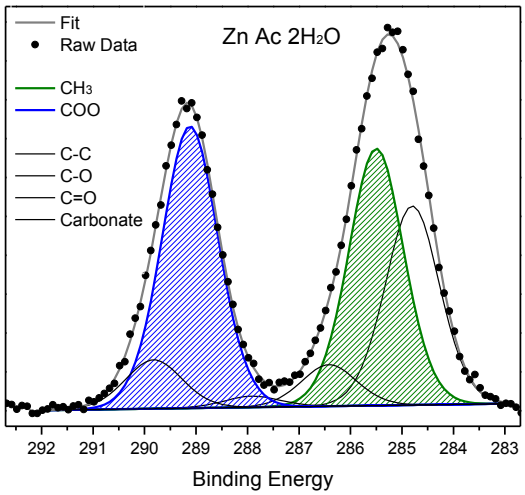

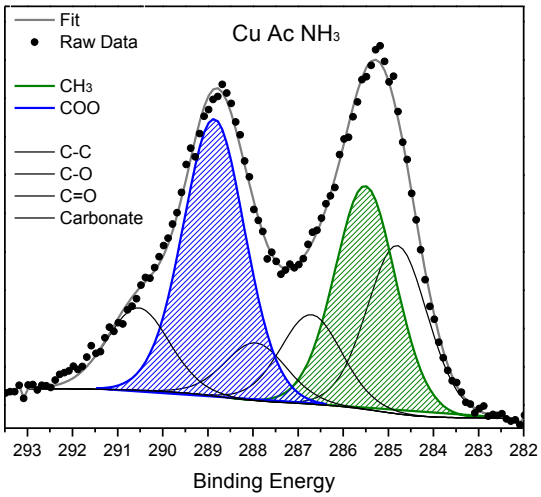

Bridging Mode

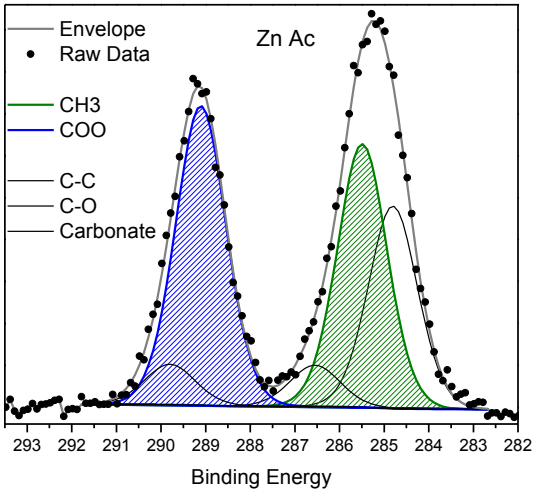

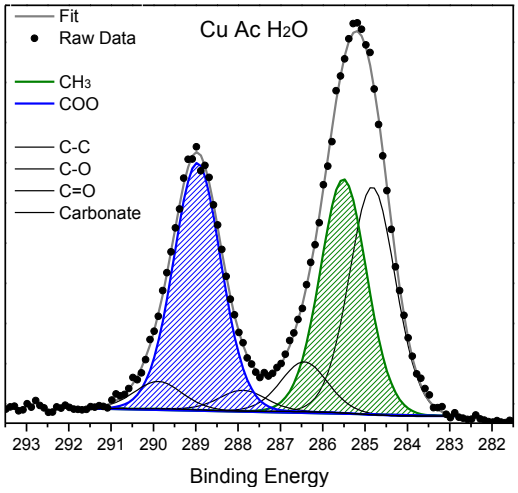

Bridging ($\mu_3\eta^1\eta^2$Mode)

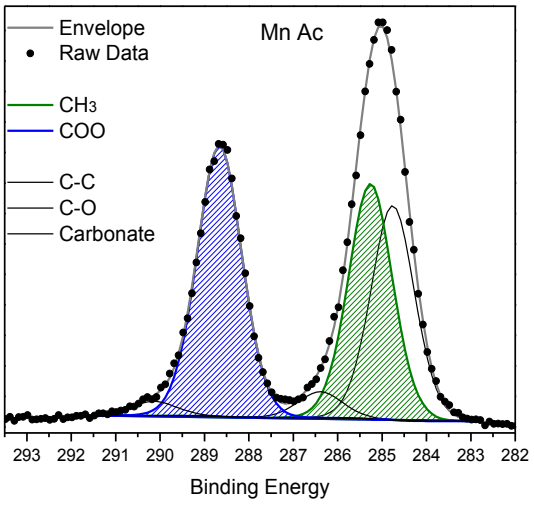

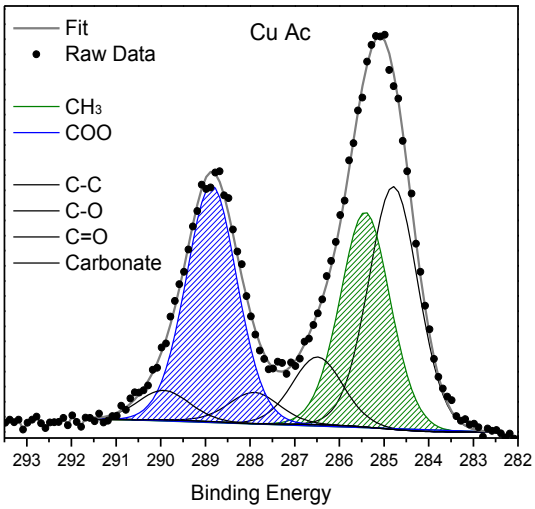

Chelating Bridging

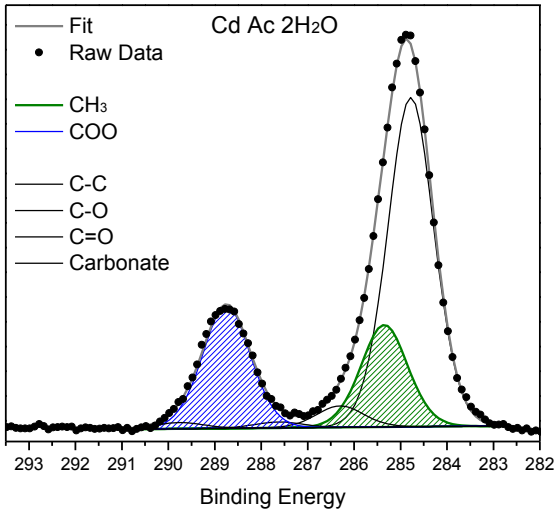

Chelating Bridging ($\mu_3\eta^1\eta^2\eta^1$Mode)

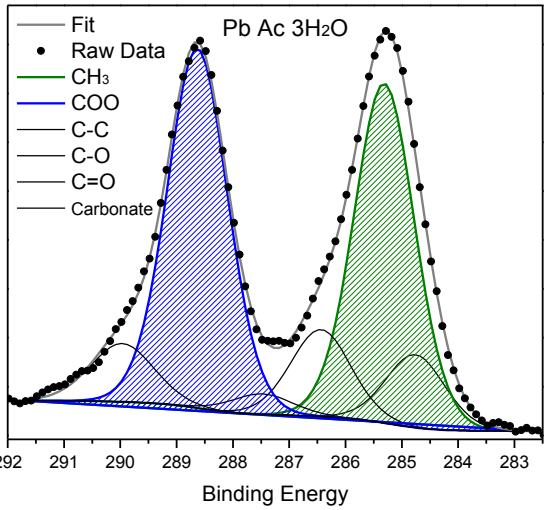

Ionic

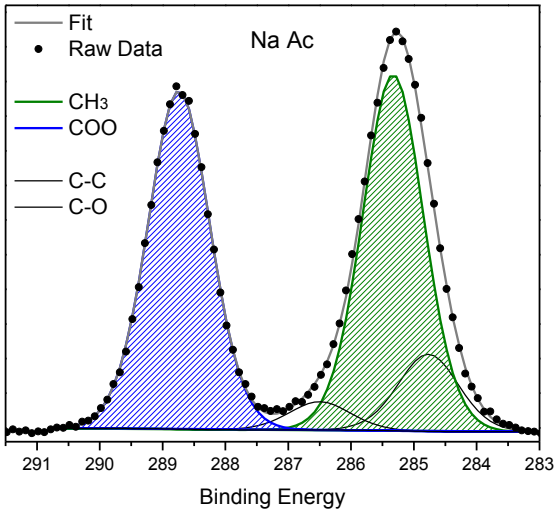

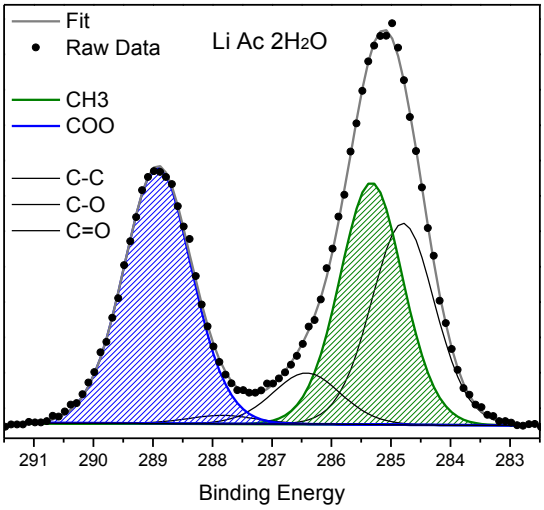

O1s Region

Pseudo Bridging Bidentate Mode

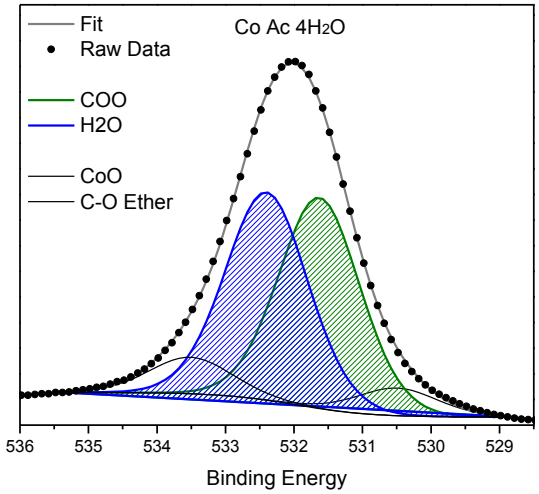

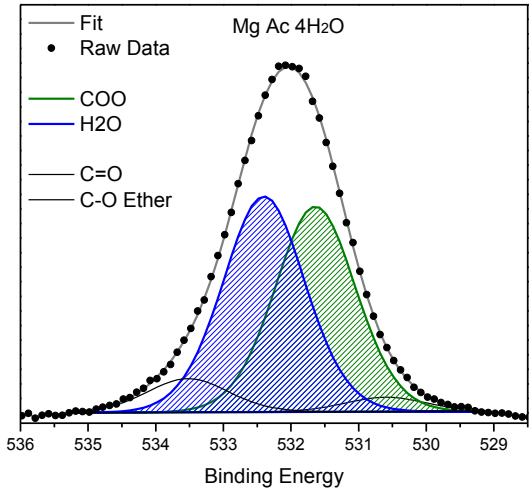

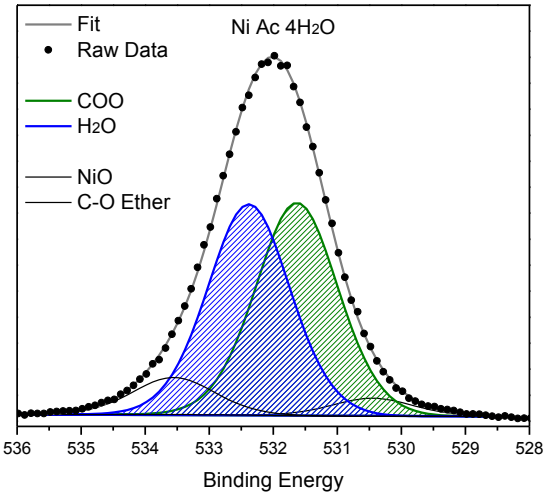

Monodentate Mode

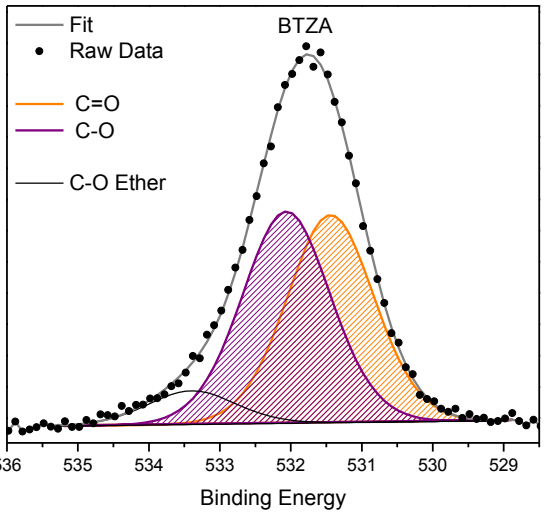

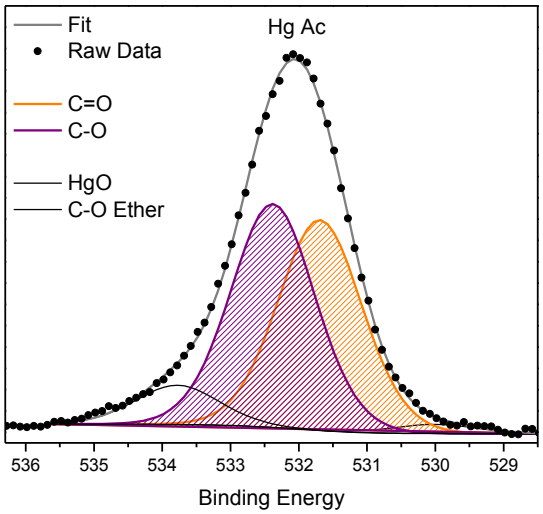

Chelating Mode

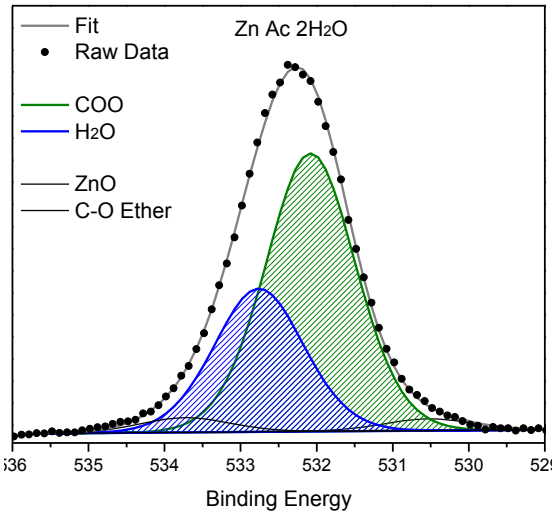

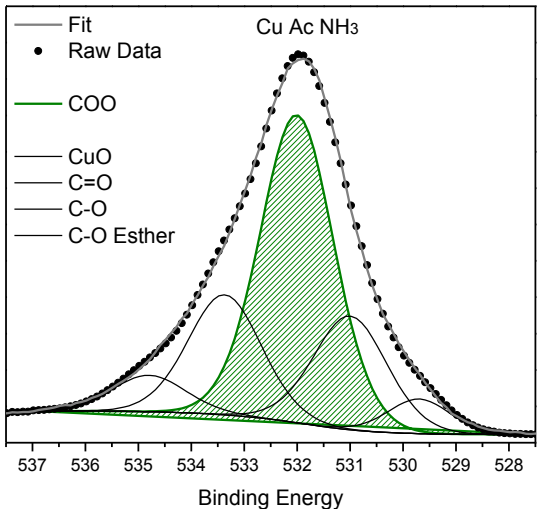

Bridging Mode

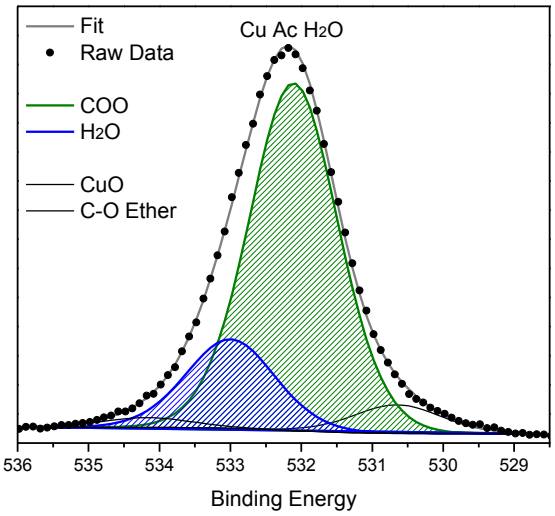

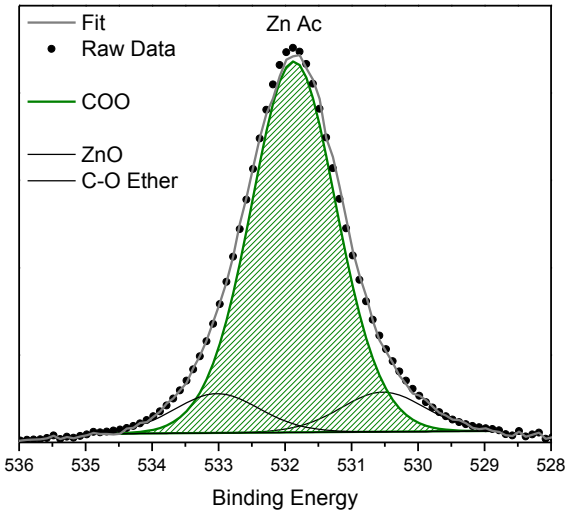

Bridging ($\mu_3\eta^1\eta^2$Mode)

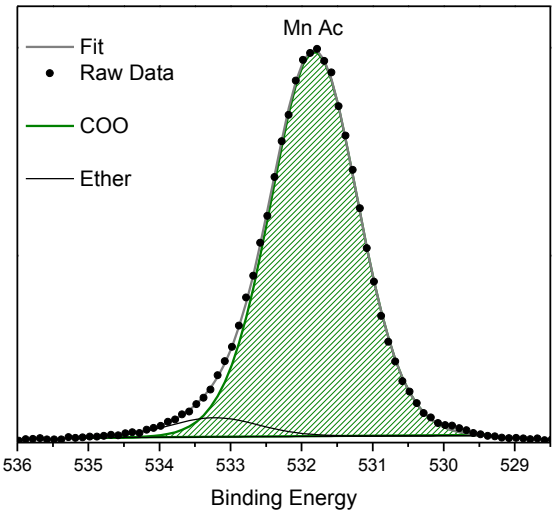

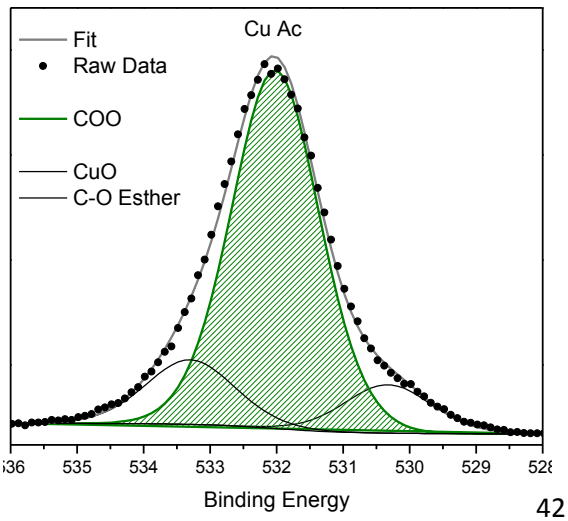

Chelating Bridging

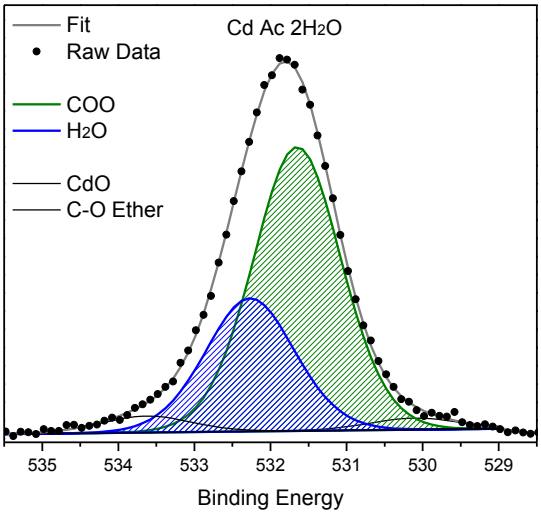

Chelating Bridging ($\mu_3\eta^1\eta^2\eta^1$Mode)

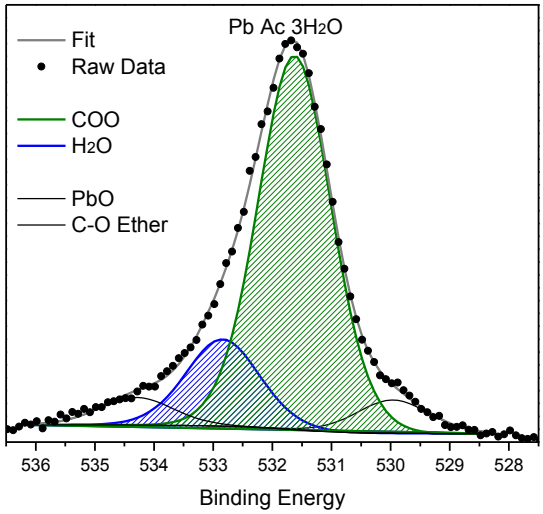

Ionic

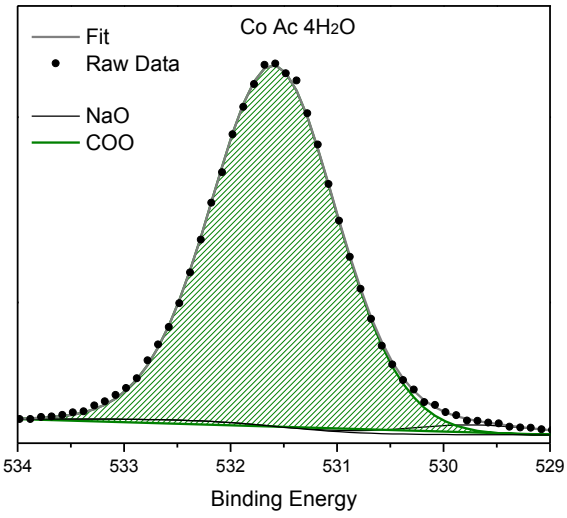

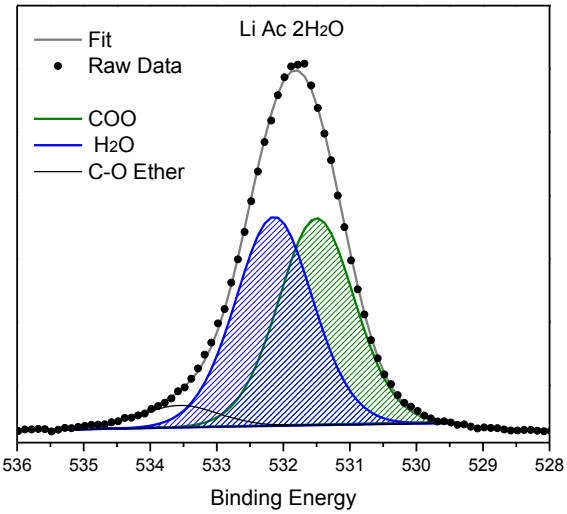

REFERENCES

1. Zaera, F., *The Surface Chemistry of Catalytic Reactions: Progress and Challenges.* The Journal of Physical Chemistry Letters, 2015. **6**(20): p. 4115-4116.
2. Jia, X., et al., *Carboxylic acid-modified metal oxide catalyst for selectivity-tunable aerobic ammoxidation.* Nature Communications, 2018. **9**(1): p. 933.
3. Dwivedi, D., K. Lepková, and T. Becker, *Carbon steel corrosion: a review of key surface properties and characterization methods.* RSC Advances, 2017. **7**(8): p. 4580-4610.
4. Frankel, G.S., et al., *A comparative review of the aqueous corrosion of glasses, crystalline ceramics, and metals.* npj Materials Degradation, 2018. **2**(1): p. 15.
5. Bai, Y., et al., *Engineering the surface charge states of nanostructures for enhanced catalytic performance.* Materials Chemistry Frontiers, 2017. **1**(10): p. 1951-1964.
6. Mohtasebi, A. and P. Kruse, *Chemical sensors based on surface charge transfer*, in *Physical Sciences Reviews*. 2018.
7. Ladomenou, K., et al., *The importance of various anchoring groups attached on porphyrins as potential dyes for DSSC applications.* RSC Advances, 2014. **4**(41): p. 21379-21404.
8. Moschona, A., et al., *Corrosion protection of carbon steel by tetraphosphonates of systematically different molecular size.* Corrosion Science, 2018. **145**: p. 135-150.
9. Shen, L., et al., *High-performance thin-film composite membranes with surface functionalization by organic phosphonic acids.* Journal of Membrane Science, 2018. **563**: p. 284-297.
10. Wilson, D. and M.A. Langell, *XPS analysis of oleylamine/oleic acid capped Fe3O4 nanoparticles as a function of temperature.* Applied Surface Science, 2014. **303**: p. 6-13.
11. Liu, J.-f., Z.-s. Zhao, and G.-b. Jiang, *Coating Fe3O4 Magnetic Nanoparticles with Humic Acid for High Efficient Removal of Heavy Metals in Water.* Environmental Science & Technology, 2008. **42**(18): p. 6949-6954.
12. Wong, K.K., et al., *Removal of Cu and Pb by tartaric acid modified rice husk from aqueous solutions.* Chemosphere, 2003. **50**(1): p. 23-28.
13. Al-Johani, H., et al., *The structure and binding mode of citrate in the stabilization of gold nanoparticles.* Nature Chemistry, 2017. **9**: p. 890.
14. Anselmi, C., et al., *Adsorption of organic dyes on TiO2 surfaces in dye-sensitized solar cells: interplay of theory and experiment.* Physical Chemistry Chemical Physics, 2012. **14**(46): p. 15963-15974.
15. Han, R., et al., *Toward interfacing organic semiconductors with ferromagnetic transition metal substrates: enhanced stability via carboxylate anchoring.* Chemical Communications, 2016. **52**(63): p. 9805-9808.
16. Khalil, M., et al., *Non-aqueous modification of synthesized hematite nanoparticles with oleic acid.* Colloids and Surfaces A: Physicochemical and Engineering Aspects, 2014. **453**: p. 7-12.
17. Pastore, M. and F. De Angelis, *Computational modelling of TiO2 surfaces sensitized by organic dyes with different anchoring groups: adsorption modes, electronic structure and implication for electron injection/recombination.* Physical Chemistry Chemical Physics, 2012. **14**(2): p. 920-928.

18. Zhang, F., et al., *Precise Identification and Manipulation of Adsorption Geometry of Donor–π–Acceptor Dye on Nanocrystalline TiO2 Films for Improved Photovoltaics.* ACS Applied Materials & Interfaces, 2014. **6**(24): p. 22359-22369.
19. Lin, S.-J., et al., *Molecular Structures of Ge(tpp)(OAc)2 and In(tpp)(OAc) and Their Implications: Correlations between the 13C NMR Chemical Shift of the Acetato Ligand and Different Types of Carboxylate Coordination in M(por)(OAc)n {por = tpp (5,10,15,20-Tetraphenylporphyrinate), tmpp (5,10,15,20-Tetrakis(4-methoxyphenyl)porphyrinate), tpyp (5,10,15,20-Tetrakis(4-pyridyl)porphyrinate); M = Ga, In, Tl, Ge, Sn; n = 1, 2}.* Inorganic Chemistry, 1997. **36**(18): p. 3886-3891.
20. Ye, B.-H., et al., *Synthesis and Structural Characterization of Di- and Tetranuclear Zinc Complexes with Phenolate and Carboxylate Bridges. Correlations between 13C NMR Chemical Shifts and Carboxylate Binding Modes.* Inorganic Chemistry, 2002. **41**(24): p. 6426-6431.
21. Muñoz Noval, Á., et al., *Coordination and structure of Ca(II)-acetate complexes in aqueous solution studied by a combination of Raman and XAFS spectroscopies.* Journal of Molecular Structure, 2018. **1161**: p. 512-518.
22. Yang, M.M., D.A. Crerar, and D.E. Irish, *A Raman spectroscopic study of lead and zinc acetate complexes in hydrothermal solutions.* Geochimica et Cosmochimica Acta, 1989. **53**(2): p. 319-326.
23. Deacon, G.B. and R.J. Phillips, *Relationships between the carbon-oxygen stretching frequencies of carboxylato complexes and the type of carboxylate coordination.* Coordination Chemistry Reviews, 1980. **33**(3): p. 227-250.
24. Zeleňák, V., Z. Vargová, and K. Györyová, *Correlation of infrared spectra of zinc(II) carboxylates with their structures.* Spectrochimica Acta Part A: Molecular and Biomolecular Spectroscopy, 2007. **66**(2): p. 262-272.
25. Akbari, A., et al., *Identification of the dye adsorption modes in dye-sensitised solar cells with X-ray spectroscopy techniques: a computational study.* Physical Chemistry Chemical Physics, 2015. **17**(16): p. 10849-10855.
26. Thomas, A.G., et al., *Adsorption of bi-isonicotinic acid on anatase TiO2(101) and (001) studied by photoemission and NEXAFS spectroscopy.* Surface Science, 2005. **592**(1): p. 159-168.
27. Hüfner, S., *Photoelectron Spectroscopy Principles and Applications*. 3 ed. Advanced Texts in Physics. 2003: Springer, Berlin, Heidelberg. 662.
28. Watts, J.F. and J. Wolstenholme, *An Introduction to Surface Analysis by XPS and AES*. 2003: John Wiley & Sons.
29. Hofmann, S., *Auger- and X-Ray Photoelectron Spectroscopy in Materials Science*. 2013, Springer-Verlag Berlin Heidelberg. p. 528.
30. Hesse, R., T. Chassé, and R. Szargan, *Peak shape analysis of core level photoelectron spectra using UNIFIT for WINDOWS*. Vol. 365. 1999. 48-54.
31. Beamson, G. and D. Briggs, *High Resolution XPS of Organic Polymers: The Scienta ESCA300 Database* Journal of Chemical Education, 1993. **70**(1): p. A25.
32. Grzelak, A., et al., *Anomalous chemical shifts in X-ray photoelectron spectra of sulfur-containing compounds of silver (I) and (II).* Journal of Electron Spectroscopy and Related Phenomena, 2015. **202**: p. 38-45.
33. Yano, T., et al., *Anomalous chemical shifts of Cu 2p and Cu LMM Auger spectra of silicate glasses.* Journal of Electron Spectroscopy and Related Phenomena, 2003. **131-132**: p. 133-144.

34. Kaden, W.E., et al., *Understanding surface core-level shifts using the Auger parameter: A study of Pd atoms adsorbed on ultrathin SiO${}_{2}$ films.* Physical Review B, 2014. **89**(11): p. 115436.
35. Moretti, G., *The Wagner plot and the Auger parameter as tools to separate initial- and final-state contributions in X-ray photoemission spectroscopy.* Surface Science, 2013. **618**: p. 3-11.
36. Moretti, G., et al., *Auger parameter and Wagner plot studies of small copper clusters.* Surface Science, 2016. **646**: p. 298-305.
37. Muñoz-Márquez, M.A., et al., *Composition and Evolution of the Solid-Electrolyte Interphase in Na2Ti3O7 Electrodes for Na-Ion Batteries: XPS and Auger Parameter Analysis.* ACS Applied Materials & Interfaces, 2015. **7**(14): p. 7801-7808.
38. D. Wagner, C., *Chemical Shifts of Auger Lines, and the Auger Parameter*. Vol. 60. 1975.
39. Moretti, G., *Auger parameter and Wagner plot in the characterization of chemical states by X-ray photoelectron spectroscopy: A review*. Vol. 95. 1998. 95-144.
40. Moulder, J.F. and J. Chastain, *Handbook of X-ray Photoelectron Spectroscopy: A Reference Book of Standard Spectra for Identification and Interpretation of XPS Data*. 1992: Physical Electronics Division, Perkin-Elmer Corporation.
41. Biesinger, M.C., et al., *Resolving surface chemical states in XPS analysis of first row transition metals, oxides and hydroxides: Cr, Mn, Fe, Co and Ni.* Applied Surface Science, 2011. **257**(7): p. 2717-2730.
42. Bravo Sanchez, M., et al., *Composition assessment of ferric oxide by accurate peak fitting of the Fe 2p photoemission spectrum.* Surface and Interface Analysis, 2017. **49**(4): p. 253-260.
43. Cabrera-German, D., et al., *Detailed peak fitting analysis of the Zn 2p photoemission spectrum for metallic films and its initial oxidation stages.* Surface and Interface Analysis, 2017. **49**(11): p. 1078-1087.
44. Gardella, J., S. A. Ferguson, and R. L. Chin, *$\pi^* \leftarrow \pi$ Shakeup Satellites for the Analysis of Structure and Bonding in Aromatic Polymers by X-Ray Photoelectron Spectroscopy*. Vol. 40. 1986. 224-232.
45. Keane, M.P., et al., *Experimental and theoretical study of the N1s and C1s shake-up satellites in pyridine and aniline.* Chemical Physics, 1991. **155**(3): p. 379-387.
46. *XPS Interpretation of Copper*. May 21, 2019]; Available from: https://xpssimplified.com/elements/copper.php.
47. Ni, M. and B.D. Ratner, *Differentiation of Calcium Carbonate Polymorphs by Surface Analysis Techniques - An XPS and TOF-SIMS study.* Surface and interface analysis : SIA, 2008. **40**(10): p. 1356-1361.
48. Kimata, M., T. Hatta, and N. Nishida, *Probing the chemical structures of silica polymorphs by X-ray photoelectron spectroscopy: The differences in Si2p and O1s binding energy between eclipsed and staggered Si2O7 configurations*. Vol. 10. 1999. 433-452.
49. Cano, A., et al., *Contribution to the coordination chemistry of transition metal nitroprussides: a cryo-XPS study.* New Journal of Chemistry, 2019. **43**(12): p. 4835-4848.
50. Batten, S.R., S.M. Neville, and D.R. Turner, *Coordination Polymers: Design, Analysis and Application*. 2008: The Royal Society of Chemistry.
51. Rardin, R.L., W.B. Tolman, and S.J. Lippard, *Monodentate carboxylate complexes and the carboxylate shift: implications for polymetalloprotein structure and function.* New J. Chem, 1991. **15**(6): p. 417-430.

52. Kadam, S.R., et al., *A green process for efficient lignin (biomass) degradation and hydrogen production via water splitting using nanostructured C, N, S-doped ZnO under solar light.* RSC Advances, 2014. **4**(105): p. 60626-60635.
53. Euler, H., et al., *Refinement of crystal structure of copper acetate diammine, Cu(CH3COO)2 · 2NH3*, in *Zeitschrift für Kristallographie - New Crystal Structures*. 2009. p. 725.
54. Barr, T.L. and S. Seal, *Nature of the use of adventitious carbon as a binding energy standard.* Journal of Vacuum Science & Technology A, 1995. **13**(3): p. 1239-1246.
55. Funk, C., et al., *Epoxy-functionalized surfaces for microarray applications: surface chemical analysis and fluorescence labeling of surface species.* Surface and Interface Analysis, 2012. **44**(8): p. 890-894.
56. Nietzold, C., et al., *Functional group quantification on epoxy surfaces by chemical derivatization (CD)-XPS.* Surface and Interface Analysis, 2014. **46**(10-11): p. 668-672.
57. Fen-rong, L., et al., *XPS study on the change of carbon-containing groups and sulfur transformation on coal surface.* Journal of Fuel Chemistry and Technology, 2011. **39**(2): p. 81-84.
58. López, G.P., D.G. Castner, and B.D. Ratner, *XPS O 1s binding energies for polymers containing hydroxyl, ether, ketone and ester groups.* Surface and Interface Analysis, 1991. **17**(5): p. 267-272.
59. Dupin, J.-C., et al., *Systematic XPS studies of metal oxides, hydroxides and peroxides.* Physical Chemistry Chemical Physics, 2000. **2**(6): p. 1319-1324.
60. Wagner, C.D., *The NIST X-ray photoelectron spectroscopy (XPS) database*. 1991: Gaithersburg, MD : U.S. Dept. of Commerce, National Institute of Standards and Technology, 1991.